NeuroImage (2022) 119453

Contents lists available at ScienceDirect

NeuroImage

journal homepage: www.elsevier.com/locate/neuroimage

Cytoarchitecture, probability maps and segregation of the human insula

Julian Quabs[a,b,c,*], Svenja Caspers[b,c], Claudia Schöne[a], Hartmut Mohlberg[c], Sebastian Bludau[c], Timo Dickscheid[c], Katrin Amunts[a,c]

[a] C. and O. Vogt Institute for Brain Research, Medical Faculty, University Hospital Düsseldorf, Heinrich Heine University of Düsseldorf, Germany
[b] Institute for Anatomy I, Medical Faculty, Heinrich Heine University of Düsseldorf, Germany
[c] Institute of Neuroscience and Medicine (INM-1), Research Centre Jülich, Germany

ARTICLE INFO

Keywords:
Insula
Cytoarchitecture
Probability maps
Brain mapping
Cluster analysis
Human Brain Atlas

ABSTRACT

The human insular cortex supports multifunctional integration including interoceptive, sensorimotor, cognitive and social-emotional processing. Different concepts of the underlying microstructure have been proposed over more than a century. However, a 3D map of the cytoarchitectonic segregation of the insula in standard reference space, that could be directly linked to neuroimaging experiments addressing different cognitive tasks, is not yet available. Here we analyzed the middle posterior and dorsal anterior insula with image analysis and a statistical mapping procedure to delineate cytoarchitectonic areas in ten human postmortem brains. 3D-probability maps of seven new areas with granular (Ig3, posterior), agranular (Ia1, posterior) and dysgranular (Id2-Id6, middle to dorsal anterior) cytoarchitecture have been calculated to represent the new areas in stereotaxic space. A hierarchical cluster analysis based on cytoarchitecture resulted in three distinct clusters in the superior posterior, inferior posterior and dorsal anterior insula, providing deeper insights into the structural organization of the insula. The maps are openly available to support future studies addressing relations between structure and function in the human insula.

1. Introduction

The insular cortex has attracted researchers for many years, going back to the early 19th century (Reil, 1809) (Fig. 1). A large number of studies using neuroimaging and electrocortical stimulation (e.g. Stephani et al., 2011; Mazzola et al., 2019) have provided evidence that the insula is a highly multifunctional, integrational brain region (Nieuwenhuys, 2012; Gogolla, 2017; Uddin et al., 2017). Functions include interoception (Craig, 2003; Garfinkel et al., 2015; Namboodiri and Stuber, 2020), socio-emotional processing (Lamm and Singer, 2010; Gasquoine, 2014), control of salience network (Menon and Uddin, 2010; Uddin, 2015), prediction (Bossaerts, 2010; Livneh et al., 2020) as well as other cognitive (Chang et al., 2013; Bermudez-Rattoni, 2014; Woolnough et al., 2019) and sensorimotor functions (Baier et al., 2014; Hu et al., 2015; de Aquino et al., 2019). In fact, the insula is involved in the processing of most sensory modalities such as auditory (Bamiou et al., 2003), vestibular (Frank and Greenlee, 2018), gustatory (Small, 2010; Avery et al., 2020), olfactory (Veldhuizen et al., 2010), nociceptive (Segerdahl et al., 2015; Bastuji et al., 2016), thermosensory (Craig et al., 2000; Oi et al., 2017) and visual (Cera et al., 2020) information.

Different parcellations schemes of the insula have been proposed in the past based on the light microscopic approach (Brodmann, 1909; Vogt and Vogt, 1919; Rose, 1928; Brockhaus, 1940; Mesulam and Mufson, 1985; Bonthius et al., 2005; Gallay et al., 2012; Morel et al., 2013; Evrard et al., 2014). A most influential cytoarchitectonic concept has been formulated by Mesulam and Mufson (1985), who performed a comprehensive histological examination primarily on macaque brains. The authors proposed a segregation of the insula with granular, dysgranular and agranular belts, arranged in a radial, wave-like orientation around the allocortical pole region (Fig. 2A). The cytoarchitectonic characteristics change along this spatial arrangement of the sectors, such that the cell packing density in layer IV decreases from superior-posterior parts to inferior direction – the concept of the granular shift. Bonthius et al. (2005) described a similar parcellation of the human insula with a granular, dysgranular and agranular part. Others identified a higher number of cytoarchitectonic areas in human (Morel et al., 2013) and monkey brains (Gallay et al., 2012; Evrard et al., 2014; Evrard, 2019), while they adhered largely to the principle of the granular shift.

In addition to such superior-inferior gradient, recent structural in vivo MRI studies reported a differentiation between the anterior and

* Corresponding author at: Institute for Anatomy I, Medical Faculty, Heinrich Heine University of Düsseldorf, Germany.
E-mail address: julian.quabs@uni-duesseldorf.de (J. Quabs).

https://doi.org/10.1016/j.neuroimage.2022.119453.
Received 5 January 2022; Received in revised form 9 June 2022; Accepted 4 July 2022
Available online xxx.
1053-8119/© 2022 The Authors. Published by Elsevier Inc. This is an open access article under the CC BY-NC-ND license (http://creativecommons.org/licenses/by-nc-nd/4.0/)

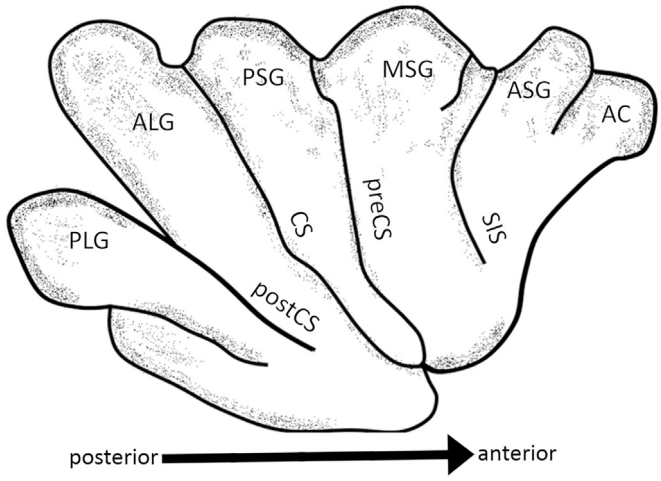

Fig. 1. Macroanatomical structure of the insular cortex modified after Clark (1896). ALG: anterior long gyrus; PLG: posterior long gyrus; PSG: posterior short gyrus; MSG: middle short gyrus; ASG: anterior short gyrus; AC: accessory gryrus; postCS: postcentral sulcus; CS: central sulcus; preCS: precentral sulcus; SIS: short insular sulcus.

posterior human insula (Menon et al., 2020; Royer et al., 2020), which has also been demonstrated in studies addressing the functional connectivity of the insular cortex in infants (Alcauter et al., 2015) and adults (Cauda et al., 2011). This additional anterior-to-posterior segregation is supported by various study results from functional meta- and connectivity analyses, which show a division of the insular cortex into three (ventral anterior, dorsal anterior, posterior) (Deen et al., 2011) to four (ventral, dorsal anterior, middle, posterior to middle) (Kurth et al., 2010a; Nomi et al., 2016) domains.

It was further assumed that both the posterior and the anterior insula are associated with different functions. The anterior insula is involved in a variety of higher cognitive and emotional processes, such as attention (Uddin, 2015; Wang et al., 2019; Cazzoli et al., 2021), prediction error (Billeke et al., 2020; Loued-Khenissi et al., 2020) and social-emotional functions (Lamm and Singer, 2010; Lau et al., 2020; Li et al., 2020). The posterior insula, on the other hand, is activated in response to somatosensory stimuli, such as pain (Segerdahl et al., 2015; Tan et al., 2017), temperature (Oi et al., 2017) or touch (Limanowski et al., 2019), and represents interoceptive states (Gehrlach et al., 2019). In comparison, the current cytoarchitectonic parcellations of the human insular cortex (Mesulam and Mufson, 1985; Bonthius et al., 2005; Morel et al., 2013) do not readily reflect such functional anterior to posterior differentiation (Fig. 2B).

Other parcellation schemes have been proposed in the past as well (for review see Nieuwenhuys, 2012). Some of them described a clear cytoarchitectonic separation between the anterior and posterior insula. Parcellations provide a wide range of microstructural areas forming the insula, varying between two (Brodmann, 1909) and thirty-one (Rose, 1928) areas. Since such historical maps represent (simplified) 2D drawings, it remains largely unclear, whether and how the different parcellation schemes can be mapped onto each other, whether they are representing, for example, a more detailed or less fine-grained map, and/or whether differences are the result of subjective mapping criteria or intersubject differences between brains underlying the respective studies. Therefore, quantitative criteria for achieving a parcellation are mandatory (Amunts and Zilles, 2015). Furthermore, the maps should be available as an atlas in stereotaxic space, as this represents a widely used basis for comparing (micro-)structure and function (Zilles and Amunts, 2010; Amunts and Zilles, 2015; Toga et al., 2006; Devlin and Poldrack, 2007).

Based on the hypothesis that areas with differences in their cytoarchitecture also differ in function (for a review see Zilles and Amunts, 2010), we here aimed to better understand the microstructural segregation of the insula, and to identify areas that may correlate with the diverse and complex functionality. Therefore, the present study analyzed the cytoarchitecture of middle to dorsal anterior human insula in both hemispheres of ten postmortem brains, supplementing earlier work of our group of the posterior granular/adjacent dysgranular as well as the anterior insula (Kurth et al., 2010b; Grodzinsky et al., 2020), to map the extent of insular areas over their whole extent based on quantitative analysis, and to compute probabilistic cytoarchitectonic maps in stereotaxic space, in order to provide a cytoarchitectonic correlate for comparisons with brain function.

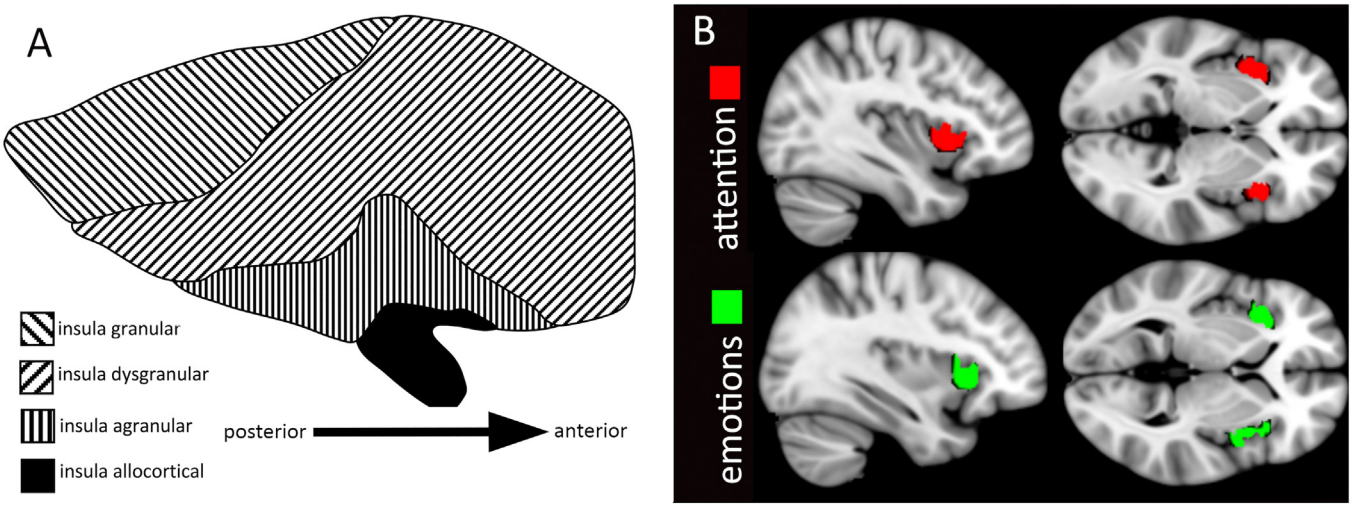

Fig. 2. (A) Microanatomical parcellation of the insula modified according to Mesulam and Mufson (1985). They described three cytoarchitectonic belts, arranged in radial, wave like orientation around an allocortical pole region: (i) one granular belt in the superior posterior to dorsal anterior insula (ii) one dysgranular belt covering the middle posterior to dorsal anterior insula (iii) one agranular belt located in the inferior posterior to ventral anterior insula. (B) A functional meta-analysis (Kurth et al., 2010a) showed, amongst others, that the anterior insula but not the posterior insula is involved in cognitive tasks such as attention or emotional processing (data downloaded from ANIMA (Reid et al., 2016)). This anterior/posterior division of the insula is not reflected by current microstructural concepts (Mesulam and Mufson, 1985; Bonthius et al., 2005; Morel et al., 2013). Mesulam and Mufson (1985), for example, described the agranular and dysgranular sector running continuously from the posterior to the anterior insula (see Fig. 2A).

Table 1
Brains used for the cytoarchitectonic analysis from the brain collection of C. and O. Vogt Institute for Brain Research, University of Düsseldorf, Germany.

Brain code	Gender	Age [years]	Brain weight [g]	Cause of death
5	Female	59	1142	Cardiorespiratory insufficiency
6	Male	54	1622	Myocardial infarction
7	Male	37	1437	Right heart failure
8	Female	72	1216	Renal failure
9	Female	79	1110	Cardiorespiratory failure
11	Male	74	1381	Myocardial infarction
12	Female	43	1198	Pulmonary embolism
17	Female	50	1328	Myocardial infarction
20	Male	65	1392	Cardiorespiratory insufficiency, carcinoma of the prostate
21	Male	30	1409	Hodgkin's disease, bronchopneumonia, deep vein thrombosis

2. Materials and methods

Cytoarchitectonic mapping has been performed in cell body-stained sections of postmortem brains. The histological processing, cytoarchitectonic analysis, mapping and alignment to 3D space followed an approach of our group that was applied in the past for many other cortical areas (Amunts et al., 2020), including previous mapping on the insula. Therefore, we only give an overview of the most important points in the following.

2.1. Histological processing of postmortem brains

Ten postmortem brains (five female, five male) within an age range from 37 to 85 years (Table 1) were obtained from body donors according to the legal and ethical conditions of the University of Düsseldorf (approval by the local Ethics Committee number #4863). None of the donors had a clinical record of neurological or psychiatric diseases. The brains were removed within about 24 h after death, and then fixed in formalin or Bodian fixative for three months or more. MR images of the formalin-fixed brains were acquired to guide the 3D reconstruction of histological sections (see below). Brains were embedded in paraffin and sectioned using a large-scale microtome (20 μm thickness). Every 15th section was stained for cell bodies using a modified silver staining method (Merker, 1983). Every 30th to 60th section (distance between sections: 0.6–1.2 mm) was analyzed from one transversally sectioned brain and nine coronally sectioned brains, in total, about 308 sections. One of the brains was the so-called Big Brain, in which each section was processed, to compute a 3D reconstruction of 20 mm (Amunts et al., 2013).

2.2. Identification of cortical borders based on the gray level index

Cortical regions of interest (ROI) were defined in images of histological sections and scanned using a CCD-Camera (Axiocam MRm, ZEISS, Germany), connected to an optical light microscope (Axioplan 2 imaging, ZEISS, Germany). The resulting high-resolution images had a spatial resolution of 1.02 um per pixel in-plane. The Gray level index (GLI) was computed in these images as a measure of the volume fraction (%) of cell bodies (Wree et al., 1982) in each measuring field (16 × 16 pixels) using an inhouse software written in Matlab (Schleicher et al., 1999; Bludau et al., 2014). The GLI images encode the cell density of each measuring field of the original image as 8bit gray value.

An inner contour line (between layer VI and the white matter) and outer contour line (between layers I and II) of the cortex were defined, and curvilinear traverses were generated between them (Schleicher et al., 1999, 2005, 2009). Gray value profiles were extracted along these traverses to capture changes in the GLI values from the surface of the cortex to the white matter boundary. I.e., GLI profiles reflect the regional cytoarchitecture (Fig. 3A). Ten features were extracted from these profiles to characterize the shape of each profile (Schleicher et al., 2009) including the mean GLI value, the center of gravity in the x-direction, the standard deviation, the skewness, the kurtosis, and the analogous parameters for the first derivative of each profile.

For determining the positions of cortical borders, significant changes between profiles in shape were detected based on the Mahalanobis distance (Mahalanobis et al., 1949) and a sliding window procedure (Schleicher et al., 2005, 2009)(Fig. 3A). Mean profiles of two adjacent blocks of profiles were compared with each other for each profile position (Fig. 3B). This resulted in a Mahalanobis distance function in dependence on the profile index (Fig. 3C). A significant maximum in this function, independent on the size of the blocks (block size between 10 and 30), indicates a change in the shape of the profiles and was used as a criterion for a cytoarchitectonic border. A border was accepted if a significant maximum (Hotelling's t-test, Bonferroni corrected, $p<0.01$) was found in three consecutive histological sections at comparable positions (Fig. 4). Every border was checked against the histological image for quality control.

2.3. Cluster analysis and multidimensional scaling analysis

The identified areas were further examined with regard to cytoarchitectonic differences and similarities by means of a hierarchical cluster analysis and multidimensional scaling analysis (MDS). To provide a comprehensive overview of cytoarchitectonic differences of the posterior and dorsal anterior insula, we also included previously mapped areas Ig1, Ig2, Id1 (Kurth et al., 2010b) of the posterior insula, and area Id7 of the dorsal anterior insula (Grodzinsky et al., 2020). Mean GLI profiles were calculated per area, brain and hemisphere, which each contained 15–20 profiles from two to three sections. The Euclidian distance (ward linkage method, (Ward, 1963)) was used to quantify differences between mean profiles of each area. The results were plotted in a dendrogram. A low Euclidian distance between areas indicates cytoarchitectonic similarities and suggests that these areas belong to a common group. In contrast, a high Euclidian distance specifies cytoarchitectonic dissimilarities and suggests different groups. In order to further quantify the microstructural features of the detected clusters on the laminar level, mean profiles for each group were calculated and described by dividing them into ten equidistant bins. The resulting profile reflects the cytoarchitectonic characteristic of the related cluster and since two of the extracted bins roughly correspond to one lamina, they can be used to study the laminar structure between the former detected groups. The multidimensional scaling analysis was used to reduce data complexity and visualize the degree of similarities or dissimilarities of each area of the insular cortex in a 2D distance matrix.

2.4. Volumetric analysis

The volume of each area was calculated, for each hemisphere and brain, and the sample was tested for sex and hemispheric differences. The volume was calculated according to the following formula based on Cavalieri's principle (Gundersen et al., 1988): $V = s$ x Δ x x Δ y x ΣNi

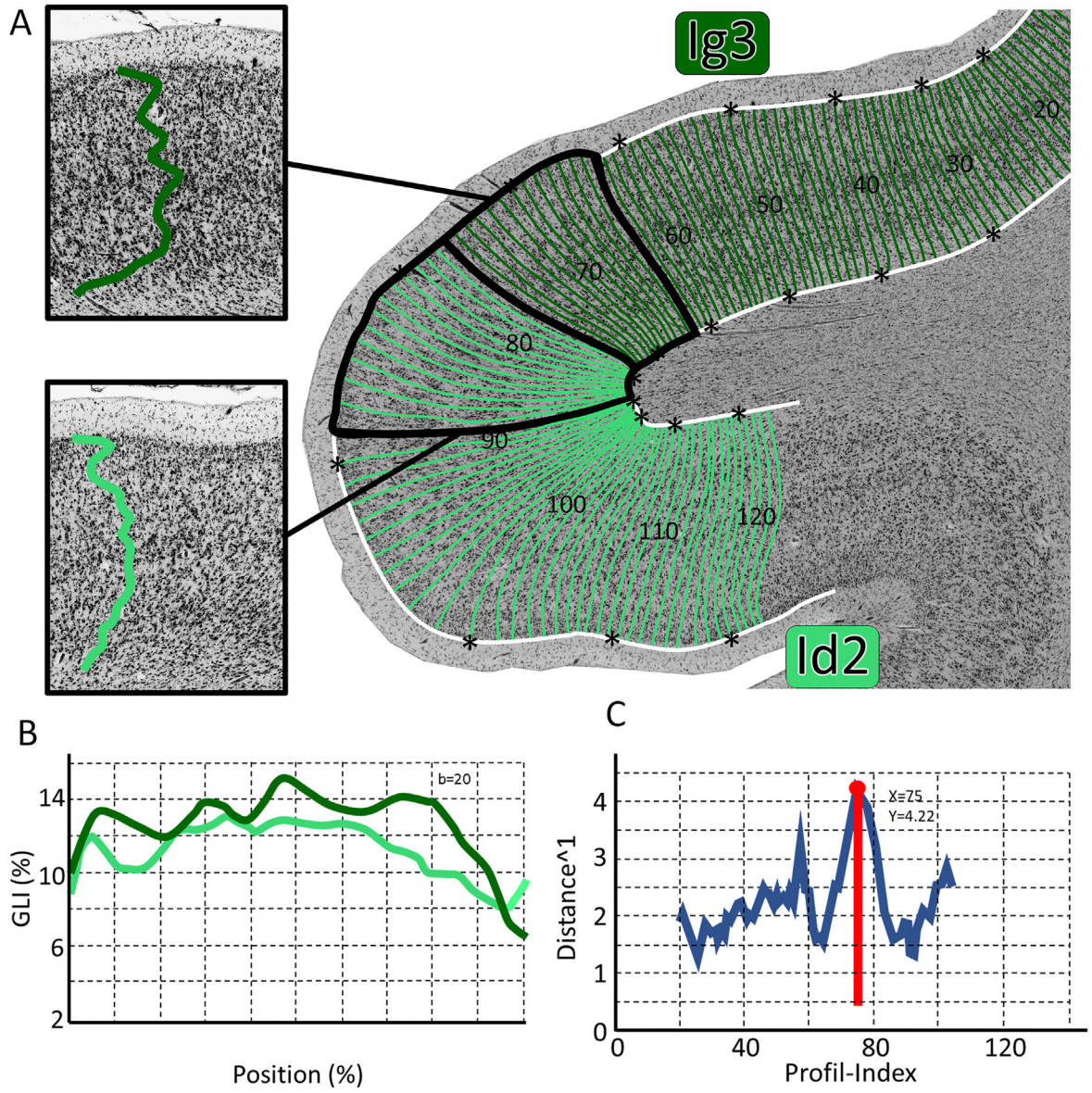

Fig. 3. Statistical detection of cortical borders. (A) A Gray Level Index (GLI) image is calculated for the region of interest (ROI), and curvilinear traverses were generated between the inner and outer contour line. Within a sliding window with two equidistant sides, mean GLI profiles are computed for each side along the traverses, representing the cytoarchitectonic composition of the corresponding cortical section. (B) Significant changes between the profile structure were measured by using the Mahalanobis distance (Mahalanobis et al., 1949). Profiles which originate from the same cytoarchitectonic area have a similar shape characterized by a low distance value. At a microstructural boundary, on the other hand, the profiles originate from different areas and therefore show different characteristics. (C) This procedure is repeated for every position of the profile index, resulting in a Mahalanobis distance function. A significant maximum in the function displays the location of a cytoarchitectonic border. In this example, the border between area Ig3 and Id2 is localized at profile position 75.

as a product of the total number of area-containing pixels (N) across every related 2D section (i), the distance between those sections (s) and the size of a single pixel (($\Delta x = \Delta y = 21.16\,\mu m$). The original volume was additionally corrected using a shrinkage factor, which is the ratio between the volume of the freshly removed brain and the volume of the histologically processed brain (Amunts et al., 2007). The volumes were normalized as ratio between volume area/total volume of the brain (in%) to make the data from different subjects comparable.

The analysis for sex and hemispheric differences was performed by a pair-wise permutation test (Bludau et al., 2014). The volumes were assorted to the corresponding group (male /female, left hemisphere/right hemisphere) and an estimated contrast was computed. The null distribution was estimated using Monte-Carlo simulation with a repetition of 1000,000 iterations. If the contrast was larger the 95% of the random distributions, we accepted the difference between groups as significant ($p = 0.05$, Bonferroni-corrected for multiple comparisons).

2.5. 3D reconstruction and interindividual variability

The identified cortical areas were 3D-reconstructed and mapped into 3D reference space using three sets of data (Amunts et al., 2020): (i) the MRI scan of the postmortem brain, performed on a 1.5-T Siemens scanner during the fixation of the brains and using a T1-weighted FLASH sequence (flip angle = 40°,repetition time = 40 ms, echo time = 5 ms), (ii) the image data set of the block faces of the paraffin-embedded brains before sectioning, and (iii) images of the stained histological sections. The combination of those data allowed us to rebuild the unprocessed histological volume for each brain. The resulting 3D reconstruction

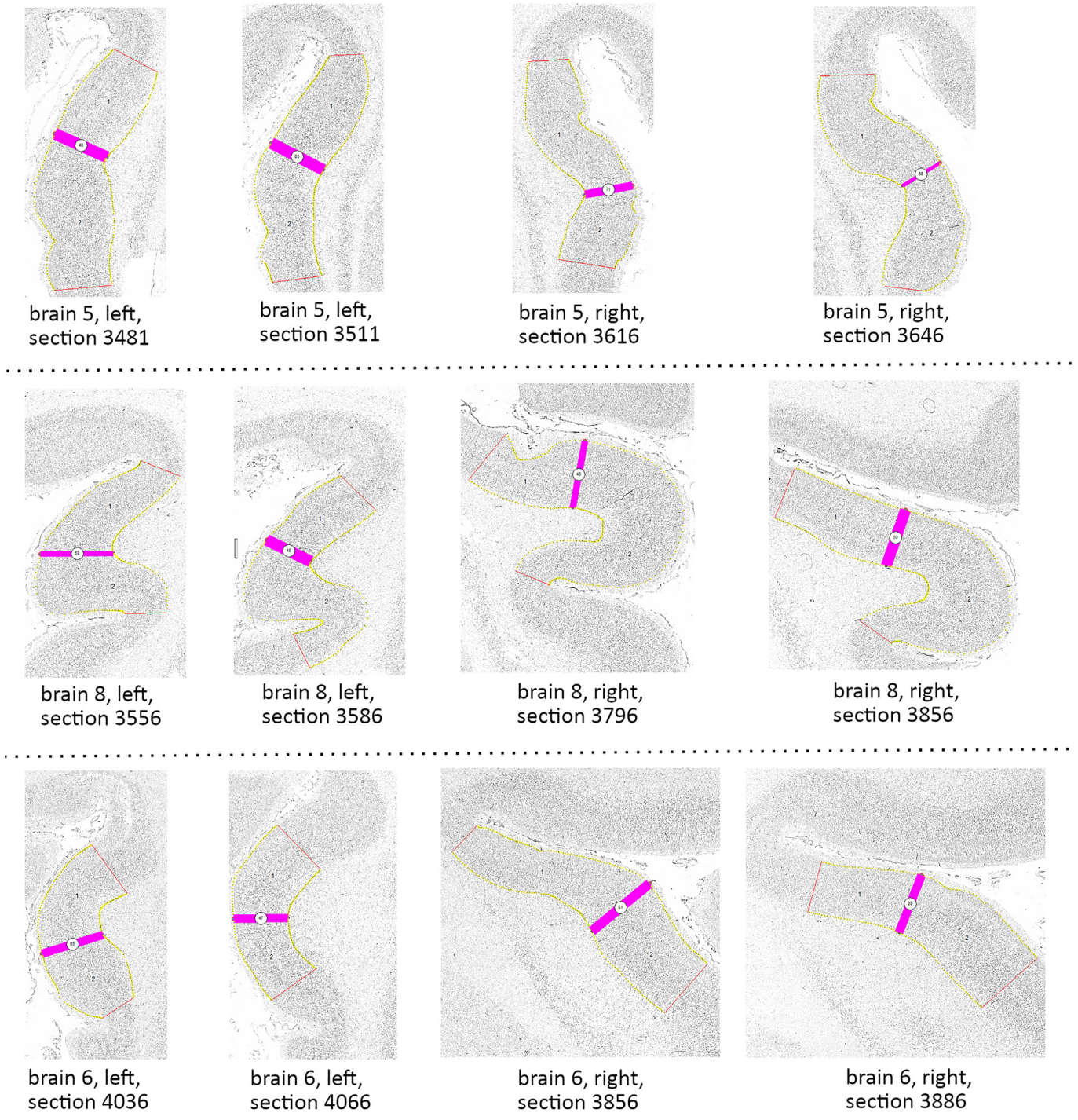

Fig. 4. Examples of statistical detection of microstructural borders. Presented here is the output of the detection algorithm, exemplified by the border between areas Ig3/Id2 for three different brains (5, 6, 8) on two slices per hemisphere. Statistical detection of borders was performed for each area on ten brains for both hemispheres. We accepted a border when it was determined on three consecutive sections at comparable positions.

was registered to the Montreal Neurological Institute (MNI) template "colin 27" (Holmes et al., 1998) and "ICBM 2009c Nonlinear Asymmetric"(Fonov et al., 2009, 2011; Evans et al., 2012) using linear and nonlinear registration tools (Hömke, 2006; Amunts et al., 2020). The data were shifted linearly by 4 mm in the y-axis and 5 mm in z-axis to make the anterior commissure the origin of our coordinate system (anatomical MNI space) (Amunts et al., 2005).

In addition, a maximum probability map (MPM) was computed, which assigns every voxel of the space to the area with the highest probability (Eickhoff et al., 2005). This procedure enables the visualization of every area at the same time without superimpositions and provides a general survey over insula's cytoarchitectonic parcellation.

These maps are openly available in the multi-modal atlas of the Human Brain Project at the EBRAINS platform (https://ebrains.eu/service/human-brain-atlas/), together with a surface map in the FreeSurfer reference space (https://ebrains.eu/news/new-maps-features-ebrains-multilevel-human-brain-atlas/).

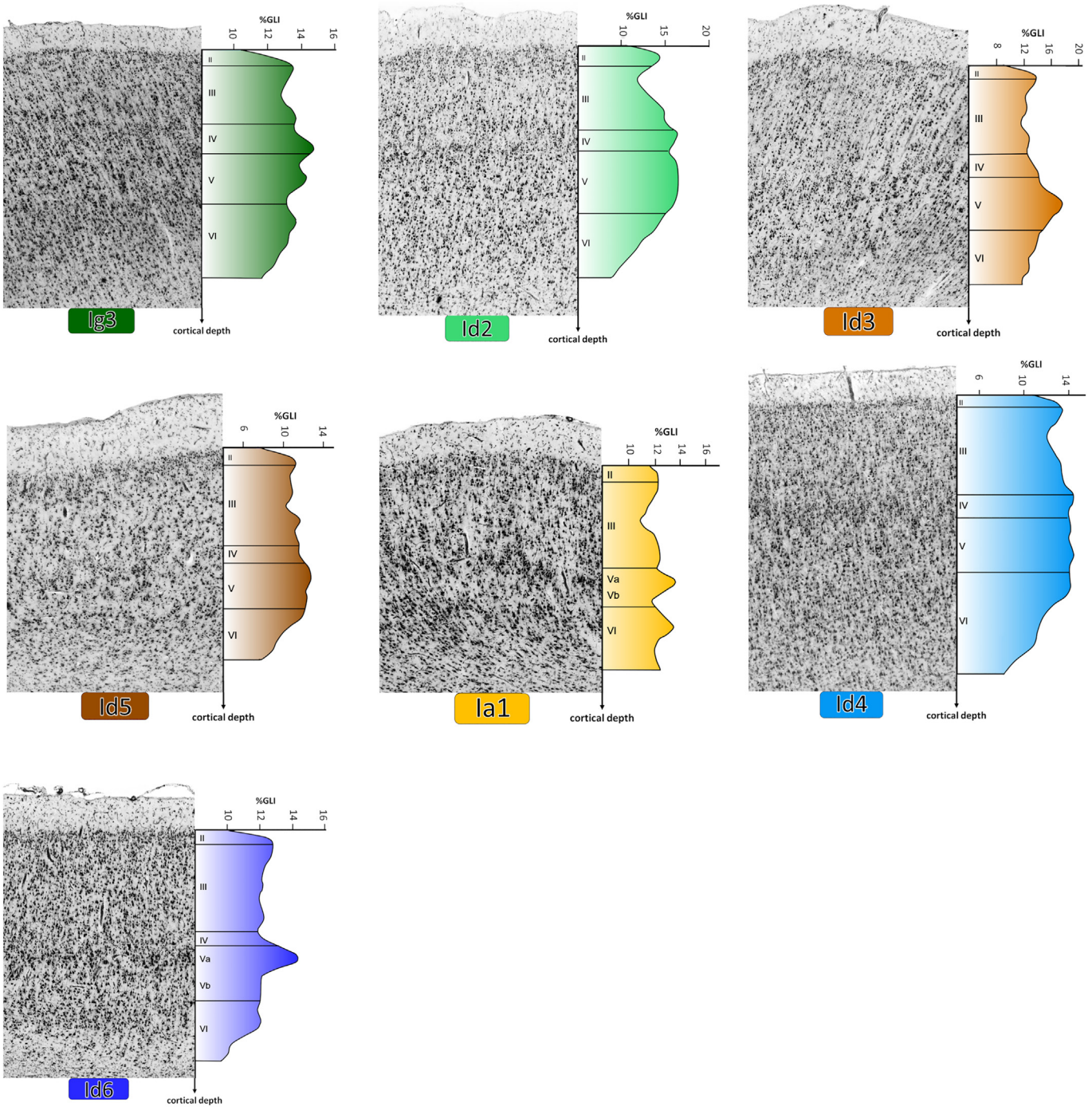

Fig. 5. Cytoarchitecture and GLI profiles of the seven newly discovered areas of the insular cortex. For a detailed microstructural description see Table 2.

3.1. Results

Seven new areas in the middle posterior to dorsal anterior insula were identified, analyzed and mapped. The areas differed in cytoarchitecture, e.g., in their granularity, i.e., the presence of layer IV. Three types of areas were distinguished: (i) layer IV was present, i.e., the area was granular (area Ig3), (ii) layer IV was present, but did not form a consistent, independent layer over its full extent, i.e., the area was dysgranular (areas Id2, Id3, Id4, Id5, Id6), and (iii) the area did not have a layer IV, i.e., the area was agranular (area Ia1). The grouping into either one of them was reflected in the name of the areas with ***I*** for insula, ***g*** for granular, ***d*** for dysgranular and ***a*** for agranular (Fig. 5, Table 2) (for more example images of the microstructural areas see Supplementary 1).

3.1.1. Cytoarchitecture of granular area Ig3

Area ***Ig3*** was characterized by a pronounced layer IV in combination with a small, compact outer granular layer II. Layers III and V contained small, evenly distributed pyramidal cells. A slightly larger layer VI with a blurred transition to the white matter and a homogenous allocation of cells complement the characteristics. In contrast, the directly adjoining granular area Ig2 (Kurth et al., 2010b) showed a broader layer II and III with a superficial-to-deep increase of cell body size, a higher peak of cell density in layer VI and a pronounced arrangement of cells in columns in layer IV (see Supplementary, Fig. 2A). The clear separation from the surrounding areas Id2 and Id4 results from a lower cell density in layer IV and different cytoarchitectonic features in layers III and V.

Table 2
Cytoarchitectonic characteristics and macroscopical localization of seven new insula areas Ig3, Ia1, Id2, Id3, Id4, Id5 and Id6.

area	cytoarchitectonic main characteristics	macroscopical localization
Ig3	-granular layer IV -small and compact layer III and V with equal distribution of cells -layer VI with blurred transition to white matter	superior part of the anterior long gyrus
Ia1	-agranular -small layer Va and VI with higher cell density compared to layer Vb resulting in a histological visible double ribbon structure -wide layer III with sparse number of pyramidal cells	inferior part of the anterior long gyrus
Id2	-wide layer II -superficial to deep increase of pyramidal cell size in layer III -homogenously distributed layer V and VI -similar to Id4, but broader layer II and smaller layer VI	middle part of the anterior long gyrus
Id3	-wide layer III with evenly distributed pyramidal cells -pronounced, dense layer V/ GLI-value outnumbering the other layers -small layer VI with clear separation to the white matter	middle part of the posterior long gyrus
Id4	-superficial to deep increase of pyramidal cell size in layer III -large pyramidal cells in layer V -wide, dense layer VI with blurred transition to white matter	superior part of the posterior short gyrus
Id5	-dense layer II -small layer V and VI in addition to wider layer III, all with homogeneous distribution of cells and low density	located on the ground of central sulcus between anterior and posterior insula
Id6	-larger, more densely packed pyramidal cells in layer Va compared to Vb resulting in clearly visible ribbon structure -wide, homogenously distributed layer III -small layer VI with clear demarcation to white matter	major proportion in the middle short gyrus, also extending to the anterior short and posterior short gyrus

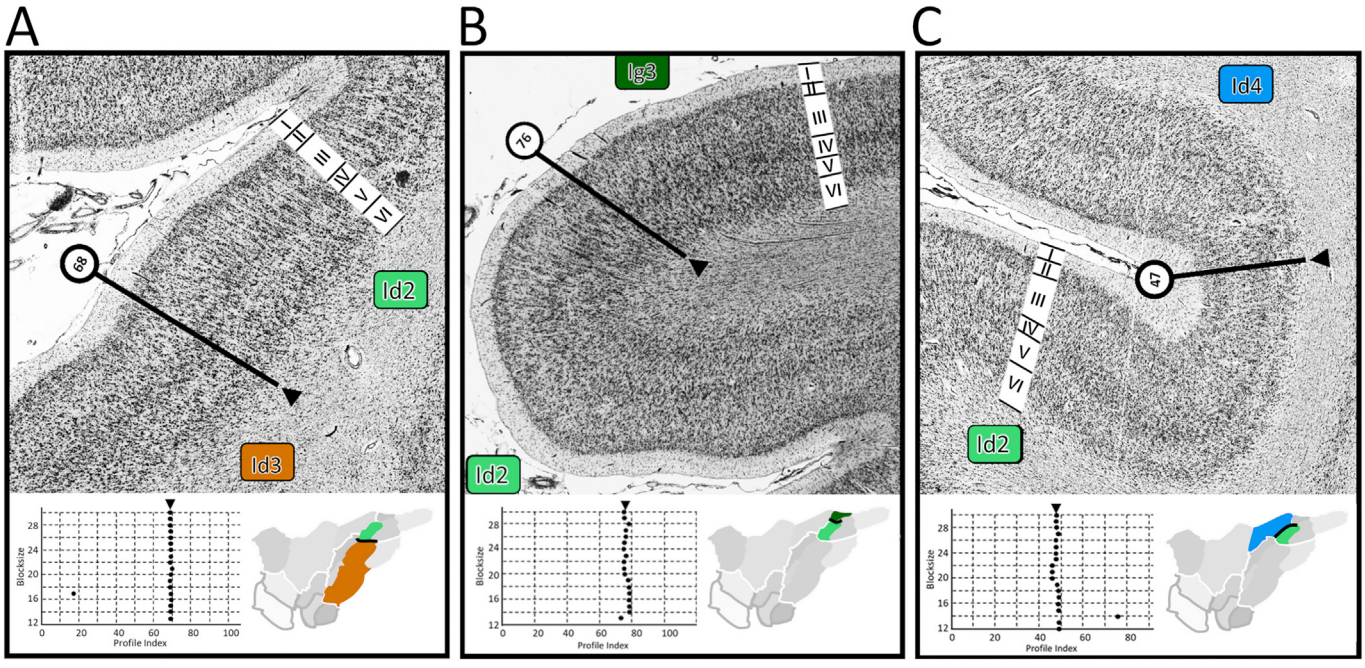

Fig. 6. Cytoarchitectonic border between (A) area Id2 and Id3; (B) area Id2 and Ig3; (C) area Id2 and Id4. The corresponding plot depicts the position of significant maxima of the Mahalanobis function across different block sizes.

3.1.2. Cytoarchitecture of dysgranular areas Id2, Id3, Id4, Id5, Id6

Area ***Id2*** comprises a wide layer II with equally distributed, small cells and a clear delimitation to the layer III. The latter showed a superficial-to-deep increase of pyramidal cell size across layer IIIa, IIIb and IIIc. Layer IV did not always form a clearly defined cortical ribbon, which made this area dysgranular. Layers V and VI were broad, with unvaryingly distribution of cell density. Image analysis and statistical testing revealed a significant border to area Ig3 (Fig. 6B) and Ig2; both areas showed a more pronounced layer IV than area Id2. Area Id4 was the anterior neighbor of Id2, and showed a similar pronounced layer IIIc, but with larger pyramidal cells. In addition, no differences of cell size between layer IIIa and IIIb and a thinner layer II were found (Fig. 6C). Moreover, area Id4 contained larger pyramidal cells in layer V than Id2.

Compared to area Id2, area ***Id3*** was composed of a thinner layer II and a wider layer III with evenly distributed cells (Fig. 6A). Layer IV was followed by a pronounced layer V, with larger cells than in area Id2 and

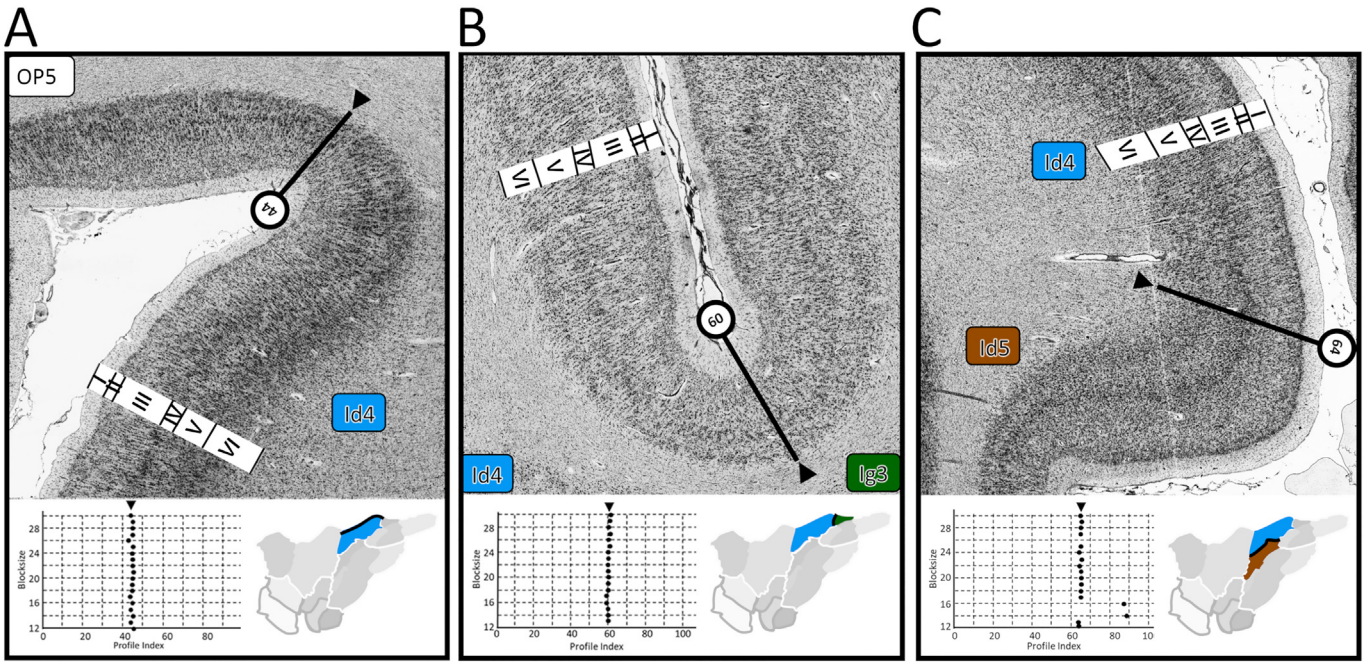

Fig. 7. Cytoarchitectonic border between (A) area Id4 and OP5; (B) area Id4 and Ig3; (C) area Id4 and Id5. The corresponding plot depicts the position of significant maxima of the Mahalanobis function across different block sizes.

a corresponding increase in the GLI, outnumbering that in other layers. Moreover, Id3 revealed a narrow layer VI with a rather clear separation to the white matter. The boundaries to the neighboring areas Ia and Id5 are discussed in detail below.

Dysgranular area ***Id4*** was mainly characterized by a dense layer V with large pyramidal cells and a broad layer III, which was further subdivided into a pronounced layer IIIc with large pyramidal cells and more loosely packed layers IIIa/b with smaller cells. Layer VI was broad as well, showed a high packing density and a blurred transition to the white matter. Layer II was narrow, densely packed, and clearly separated from layer III. The Mahalanobis distance revealed a clear peak indicating the border to posterior neighboring area Ig3 (Fig. 7B). The localization of this border coincides with the central sulcus of the insula. In contrast to area Id4, area Ig3 contains a more pronounced layer IV, equally distributed cells in layer III and a narrow layer V with smaller cells. Compared to area Id5, area Id4 showed a higher overall density of cells throughout all cortical layers, a different cellular distribution in layer III and larger pyramidal cells in layer V (Fig. 7C).

Area ***Id5*** revealed an even distribution of small cells across all layers and a low overall cell density. A thin layer II and a relatively broad layer III is followed by a weakly pronounced layer IV, which allow to distinguish this area from areas Id6 (see Supplementary, Fig. 3A), Id2, Id4 and Id3. In addition, Id5 showed a narrow layer V. The narrow layer VI was clearly separated from the white matter.

Continuing in anterior direction, area ***Id6*** was identified due to a densely packed sublayer Va, which strongly contrasts against a loosely packed layer Vb. The resulting pattern is already detectable at low magnifications and is a unique feature in human insular areas. Further attributes are a broad layer III and a narrow layer VI, both with small, homogeneously distributed cells. While the posterior neighboring area Id4 is also dysgranular with a narrow layer II, both can be distinguished by their layers III and V (Fig. 8B). In addition, area Id4 consists of a larger and more densely packed layer VI. The rostrally adjacent area Id7 (Grodzinsky et al., 2020) can be delimited, because of a significantly denser and wider layer VI as well as a denser deep layer III (Fig. 8A). The inferiorly located area Id9 (DOI: 10.25493/JMCR-ZNQ) showed a more discontinuous layer II, stronger dysgranularity close to the absence of layer IV as well as bipolar neurons in layer V. Those features permit to determine a clear statistical boundary to this area (Fig. 8C).

3.1.3. *Cytoarchitecture of agranular area Ia1*

Agranular area ***Ia1*** has three major cytoarchitectonic characteristics, distinct from neighboring dysgranular areas Id3 (Fig. 9A) and Id5 (Fig. 9C). Layer IV is hardly detectable, layers Va and VI are narrow and show a higher cell density in contrast to a sparse number of pyramidal cells in layer Vb. This microstructural pattern results in a histologically visible, unique double ribbon structure. Moreover, the small, loosely packed layer II is followed by a homogenously distributed, loosely packed layer III, which is the broadest layer in this area. A clear border to area Ia3 (DOI: 10.25493/QS00-PJ9) at the inferior, posterior insula pole derives from the clear termination of the histological double ribbon (Fig. 9B).

3.2. *Differentiation from non-insula areas*

Different areas surround the here described areas of the insular cortex in the adjacent frontoparietal operculum and the temporal lobe. Three new areas have recently been mapped in the frontoparietal operculum, which is adjacent to the insular cortex in superior direction: areas OP5 (DOI: 10.25493/HWWZ-ZBQ), OP6 (DOI: 10.25493/E0MF-GFE) and OP7 (DOI: 10.25493/CS0Y-54 J). Granular area OP5 is adjacent to insular area Id4 (Fig. 7A). Similar to dysgranular area Id4, OP5 showed a superficial-to-deep increase of cell size in a broad layer III. Nevertheless, a more clearly developed layer IV and a thinner and looser packed layer VI in area OP5 are distinct from area Id4. Area Id6 is mostly abutting to area OP7 across the circular sulcus (see Supplementary, Fig. 3B). The dysgranular opercular area OP7 showed a gradient in cell size in layer III, which was not found in area Id6 in the same way. In addition, the pronounced ribbon structure of layers Va and Vb clearly separates area Id6 from OP7. Granular area Ig3, located in the posterior, superior insula, adjoins area OP3 (Eickhoff et al., 2006) (see Supplementary, Fig. 3C). Both areas can be distinguished by a much higher density in layer IV in area Ig3 than in OP3. In posterior-inferior direction, area Id3 borders neighboring area TI (Zachlod et al., 2020) in the temporo-insular region (see Supplementary, Fig. 2B). Area TI showed a broader

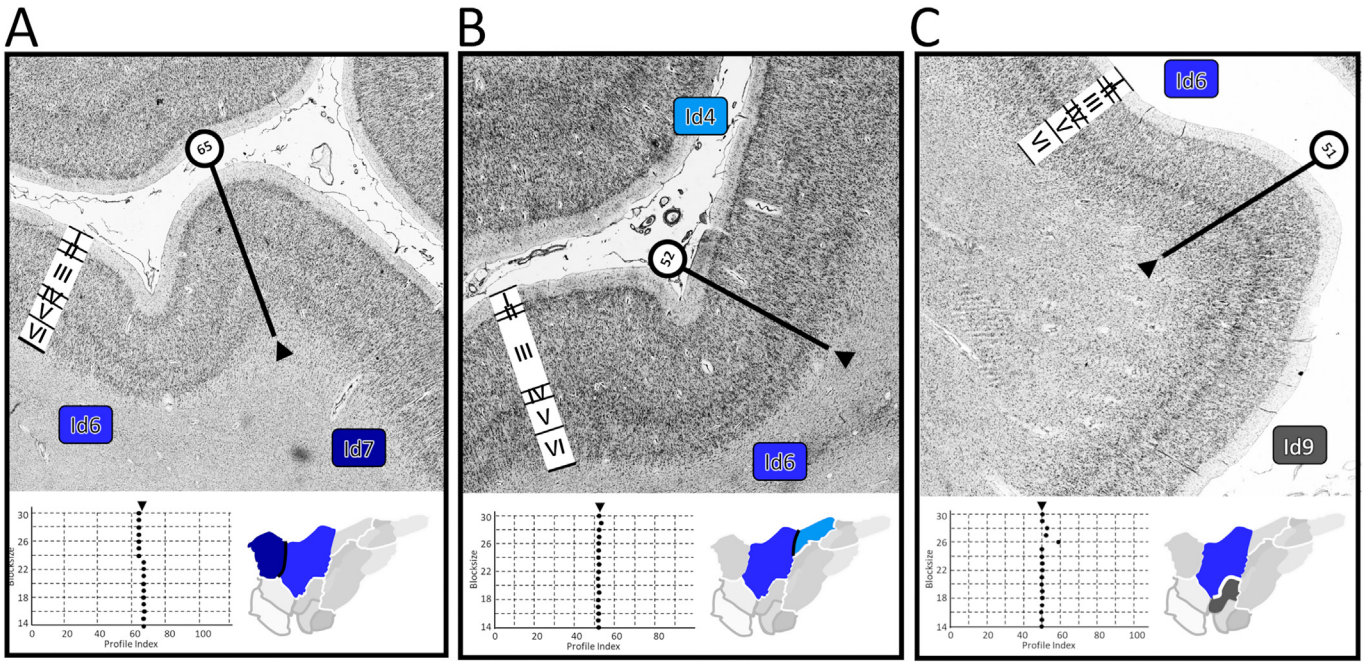

Fig. 8. Cytoarchitectonic border between (A) area Id6 and Id7; (B) area Id6 and Id4; (C) area Id6 and area Id9 (DOI:10.25493/JMCR-ZNQ). The corresponding plot depicts the position of significant maxima of the Mahalanobis function across different block sizes.

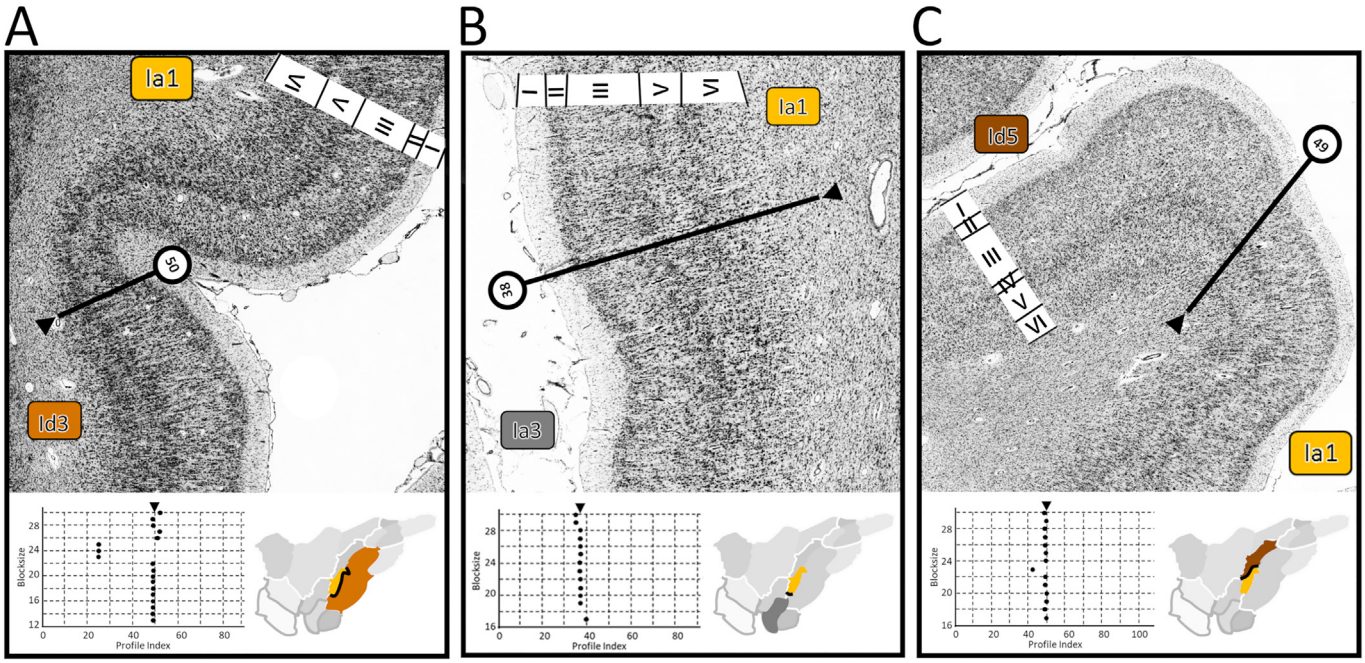

Fig. 9. Cytoarchitectonic border between (A) area Ia1 and Id3; (B) area Ia1 and area Ia3 (DOI: 10.25493/QS00-PJ9); (C) area Id5 and Ia1. The corresponding plot depicts the position of significant maxima of the Mahalanobis function across different block sizes.

layer II, and a sublamination of layer III, whereas area Id3 had a more homogenous layer III and a more pronounced layer V. The statistical analysis indicated a clear border between both areas at the fundus of the inferior, temporo-insular part of the circular sulcus.

3.3. Hierarchical cluster analysis of the posterior and dorsal anterior human insula

The hierarchical cluster analysis provided evidence for a grouping of the eleven areas of the posterior and dorsal anterior human insula into three major clusters: i) a granular-dysgranular, superior posterior cluster located in the superior posterior insula, ii) a dysgranular-agranular, inferior posterior cluster in the middle posterior to inferior insula, and iii) a dysgranular, dorsal anterior cluster covering the posterior short, middle short and anterior short gyrus (Fig. 10A). The central sulcus was identified as the dividing landmark between the anterior and posterior domains, whereas area Id5 was mostly localized in the sulcus ground, which was therefore assigned to the areas of the posterior insula.

The granular-dysgranular, superior-posterior cluster is formed by areas Ig1, Ig2, Ig3 and Id2. The granular areas Ig1, Ig2 and Ig3 all contain

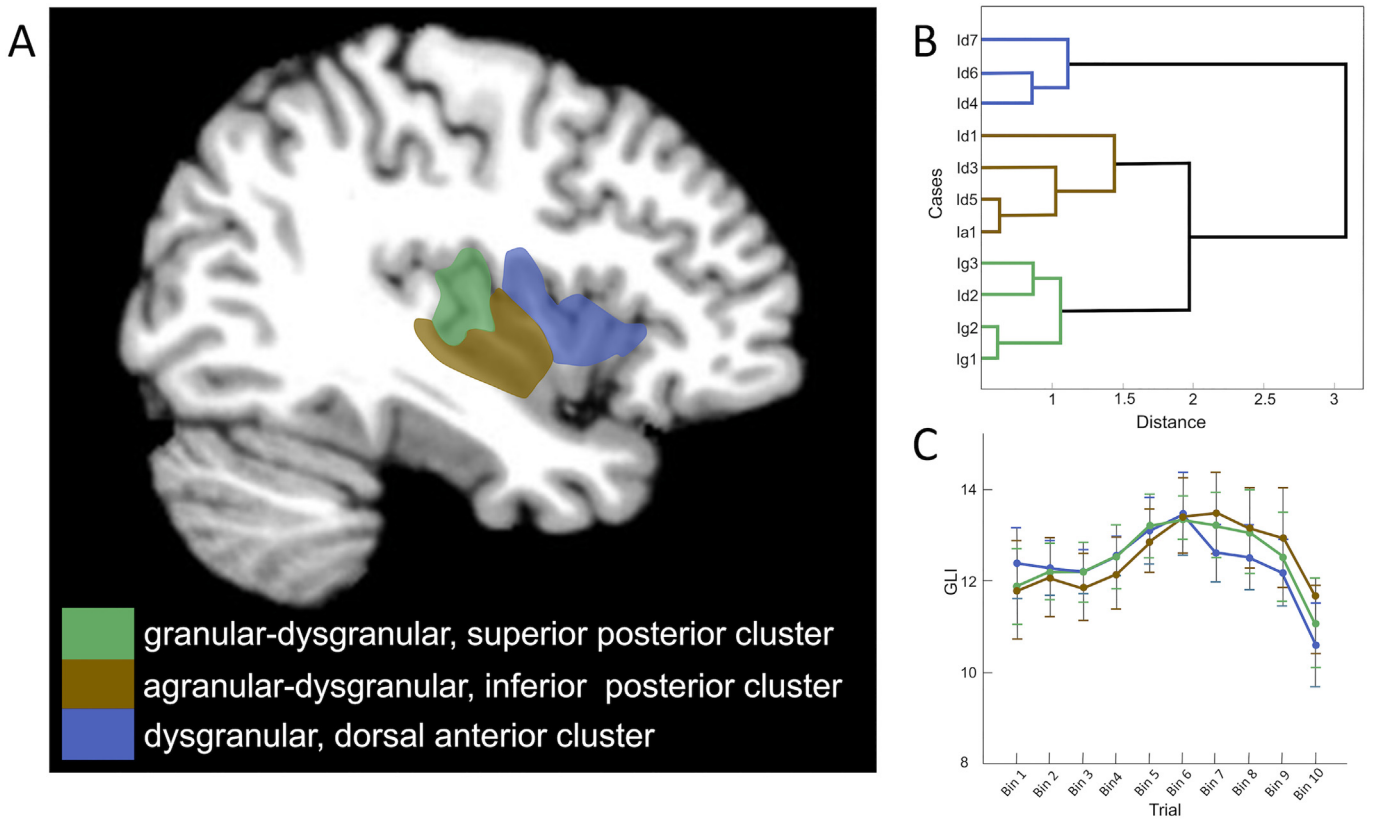

Fig. 10. (A) Hierarchical cluster analysis of seven new insula areas Ig3, Ia1, Id2, Id3, Id4, Id5 and Id6, as well as previously mapped areas Id1, Ig1, Ig2 (Kurth et al., 2010) and Id7(Grodzinsky et al., 2020). We identified three clusters: one granular-dysgranular, superior posterior cluster, one agranular-dysgranular cluster in the middle to inferior posterior insula and one dysgranular cluster in the dorsal anterior insula. Areas of the ventral insula are not included in this study. (B) The corresponding Dendrogram representing similarities and dissimilarities between areas according to the Euclidian distance. (C) Analysis of cluster-specific cytoarchitecture identified a lower density of infragranular layers for the dysgranular, dorsal anterior cluster compared with the posterior clusters. The granular-dysgranular, superior posterior cluster and the dysgranular, dorsal anterior cluster consist of a similar density of cells in the supragranular layers, whereas the agranular-dysgranular, inferior posterior cluster showed higher cellular density in the infragranular layers and lower density in the supragranular laminars.

a pronounced layer IV. Notably area Ig1 and Ig2 showed a more similar composition compared to areas Ig3 and Id2 which form a second subcluster (Fig. 10B). This observation is microstructurally reflected by a wider layer III and II of granular areas Ig1 and Ig2, as well as a more pronounced layer IV. Although dysgranular area Id2 has a less prominent layer IV, there is a clear structural similarity to area Ig3, especially in the infragranular layers.

The dysgranular-agranular, inferior-posterior group consists of area Ia1, Id1, Id3 and Id5. The layer specific analysis using the grouped mean profiles revealed a lower density of the supraganular layers, but a higher density of the infragranular layers in comparison to the granular-dysgranular, superior posterior and dysgranular, dorsal anterior cluster (Fig. 10C). The agranular area Ia1 with its unique double ribbon structure differs from the dysgranular areas, although it is more alike to area Id5. Area Id1 and Id3 are both located in the circular sulcus of the insula and showed homogeneous distribution of cells in all layers. Nevertheless, area Id1 was structurally the most dissimilar area in the dysgranular-agranular inferior posterior cluster.

The dysgranular, dorsal-anterior cluster is characterized by a lower density in the infragranular layers and a higher density in the supraganular layers compared to the dysgranular-agranular, inferior posterior neighbor. Furthermore, the layer specific analysis based on the mean profiles exposed less compact deep layers V and VI in contrast to the granular-dysgranular, superior posterior cluster. Areas Id4 and Id6 were structurally more alike compared to area Id7.

The comparison of the mean cell density of the different clusters (Fig. 10C) provided evidence for another two microstructural gradients, in addition to the established superior to inferior decrease of density in layer IV: 1) a superior posterior to inferior decrease of cellular density in the supragranular layers, as well as an increase of density in the infragranular layers; and 2) a posterior to dorsal anterior decrease of cellular density in the infragranular layers.

The MDS shows almost identical results as compared to the cluster analysis (Fig. 11). Only area Id1 is localized between the dysgranular-agranular, inferior posterior cluster and the granular-dysgranular, superior posterior cluster and cannot be clearly assigned to one of the domains.

3.4. Volumes of areas

The analysis of mean volumes showed that area Id6 is the largest area with a shrinkage corrected mean volume of 1268.9 +/- 255.6 mm^3 (left) and 1239.1/- 267.7 mm^3(right). The smallest one is the agranular area Ia1 with a corrected mean volume of 150.6 +/- 52.6 mm^3 (left) and 173.9 +/- 54.8 mm^3 (right). The other areas vary between those volumes (Table 3). The pairwise permutation test did not show significant differences with respect to sex and hemispheric differences.

3.5. Cytoarchitectonic probability maps in stereotaxic space

Probability maps for each area in the 3D T1-weighted template of the single subject MNI space (Colin-27 reference brain) (Holmes et al., 1998) and the ICBM 2009c Nonlinear Asymmetric template (Fonov et al., 2009, 2011; Evans et al., 2012) were calculated, providing information

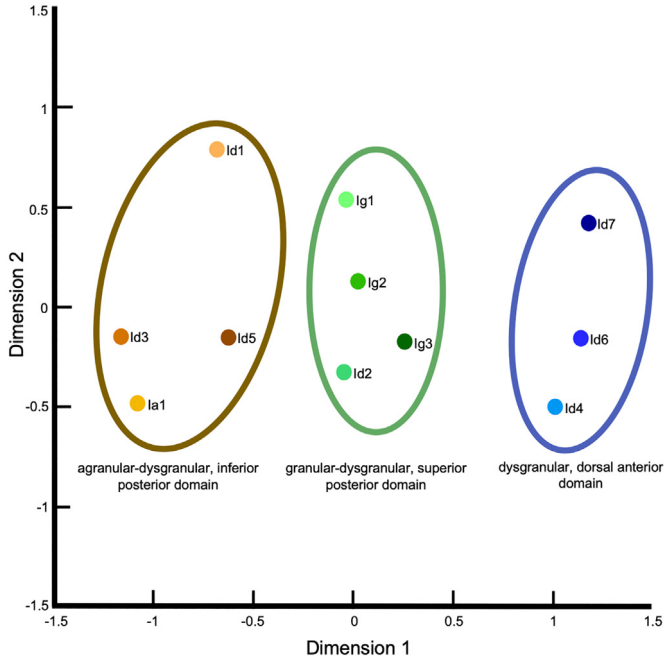

Fig. 11. Analysis of multidimensional scaling (MDS) of the eleven cytoarchitectonically distinct areas in the human insula cortex (averaged across brains and hemispheres). Except for area Id1, which was localized between the granular-dysgranular, superior posterior cluster and the agranular-dysgranular, inferior posterior domain, the MDS confirmed the results of our cluster analysis (Fig. 10). In particular, the similarities between the areas of the dorsal anterior insula as compared to the areas of the posterior insula clarify the microstructural differentiation of the posterior and anterior insula along the sulcus centralis insulae.

Table 3
Corrected mean volumes (mm3) and corresponding standard deviation (SD) of each new area of the insular cortex for the left and right hemisphere.

area	corrected mean volume [mm^3] ± SD	
	left hemisphere	right hemisphere
Ig3	228,4 ± 123,1	254,4 ± 105,2
Ia1	150,6 ± 52,6	173,9 ± 54,8
Id2	324,3 ± 133,4	315,8 ± 189,4
Id3	427,7 ± 109,7	446,4 ± 120,67
Id4	432,7 ± 177,9	410,2 ± 178,7
Id5	412,1 ± 157,8	448,4 ± 147,7
Id6	1268,9 ± 255,6	1239,1 ± 267,7

about the exact localization of the areas in stereotaxic space and their interindividual variability (Fig. 12). The centers of gravity of the areas are presented in Table 4. Area Ig3 showed the highest variability. The lowest variability was observed in area Id6.

The maximum probability map (MPM), in which every voxel is allocated to the area with the higher likelihood, reflects the relationship and topography of the microstructural areas amongst one another (Eickhoff et al., 2005) (Fig. 13). The probability maps and the MPM are publicly and freely available for download at the Julich-Brain atlas (https://jubrain.fz-juelich.de/apps/cytoviewer2/cytoviewer-maintenance.php##mitte) and the Human Brain Project (https://atlases.ebrains.eu/viewer/-/a:juelich:iav:atlas:v1.0.0:1/t:minds:core:referencespace:v1.0.0:tmp-fsaverage/p:minds:core:parcellationatlas:v1.0.0:94c1125b-b87e-45e4-901c-00daee7f2579-290/@:0.0.0.-W000..2_qztu.-8_uv.–2o6B.2_iz3G..23x6..0.0.0..1).

3.6. Topography of the insular areas

The newly available surface view of the Julich-Brain atlas allows to visualize the topographic proximity of the insular areas and the adjacent regions in more detail (Fig. 13). Granular area Ig3 is located in the superior part of the anterior long gyrus, abutting posteriorly to area Ig2 (Kurth et al., 2010b). The central sulcus of the insula represents the anterior border of Ig3 to neighboring area Id4 in all examined brains. The circular sulcus is also an approximate border to the superiorly located opercular area OP3 (Eickhoff et al., 2006) but did not reflect the exact microstructural border in all cases. Area Id2 adjoins area Ig3 in inferior direction, also abutting posteriorly to area Ig2. It mostly follows the course of the postcentral insular sulcus, covering the anterior long gyrus to a major part, whereas inferior area Id3 covers the middle part of the posterior long gyrus. Similar to posteriorly located area Id1 (Kurth et al., 2010b), Id3 extends onto the supratemporal plane next to the temporo-insular cortex. Agranular area Ia1 is located rostrally in the inferior part of the anterior long gyrus. It is bordering the inferior pole of the posterior insula. The superior adjoining area Id5 develops along the central sulcus, differentiated from posterior areas Id2 and Id3. Regarding the dorsal anterior insula, dysgranular area Id4 is located superior to Id5 in the superior part of the posterior short gyrus. Anteriorly adjacent area Id6 covers most of the dorsal anterior insula including the posterior short gyrus, the middle short gyrus and the posterior part of the anterior short gyrus. In rostral direction, area Id7 (Grodzinsky et al., 2020) completes the parcellation. The superior border of area Id6 and Id4 is approximately displayed by the circular sulcus, abutting to opercular areas OP5 and OP7. Similar to area Ig3, the circular sulcus does not reflect the microanatomical border in all cases. For further visualization of the described topography see Figs. 14 and 15.

4. Discussion

The present study provides a new cytoarchitectonic parcellation of the middle and dorsal anterior human insula in the 3D MNI reference space, based on statistical definition of borders and interindividual variability. We discovered seven new areas in the human insula with granular (Ig3), agranular (Ia1) and dysgranular (Id2-Id6) cytoarchitecture, located next to previously identified areas Ig1, Ig2, Id1 (Kurth et al., 2010b) and Id7 (Grodzinsky et al., 2020). The cluster analysis of all eleven areas provided evidence for a tripartition of the insula into i) granular-dysgranular, superior posterior cluster, ii) a dysgranular-agranular, inferior posterior cluster in the middle insula and iii) a dysgranular, dorsal anterior cluster covering the posterior, middle and anterior short gyrus (Figs. 10 and 13).

4.1. The human insula - general cytoarchitectonic principles

The granular shift is a well-established, superordinate cytoarchitectonic principle of the insula (Mesulam and Mufson, 1985). However, our study provides strong evidence to expand this classical microstructural concept of the insular cortex. While the cytoarchitectonic analysis confirms the existence of the granular shift, the cluster analysis also reveals that the overarching changes in microstructure of the insula are not only dependent on the presence of layer IV. In addition, a general increase in density in the infragranular layers and a decrease in the supragranular layers could be observed when analyzing areas from posterior, superior to posterior, inferior direction (Fig. 10C). Moreover, there was a clear decrease in density in the infragranular layers of the dorsal anterior domain compared to the posterior clusters (Fig. 10C). Therefore, the present study provides evidence to consider the overall dysgranular part of the human insula as dichotomous, separated by the central sulcus, and not as uniform (Fig. 10A).

In comparison to the cluster analysis, the MDS yields almost identical results (Fig. 11). Only area Id1 is not clearly associated with one of the

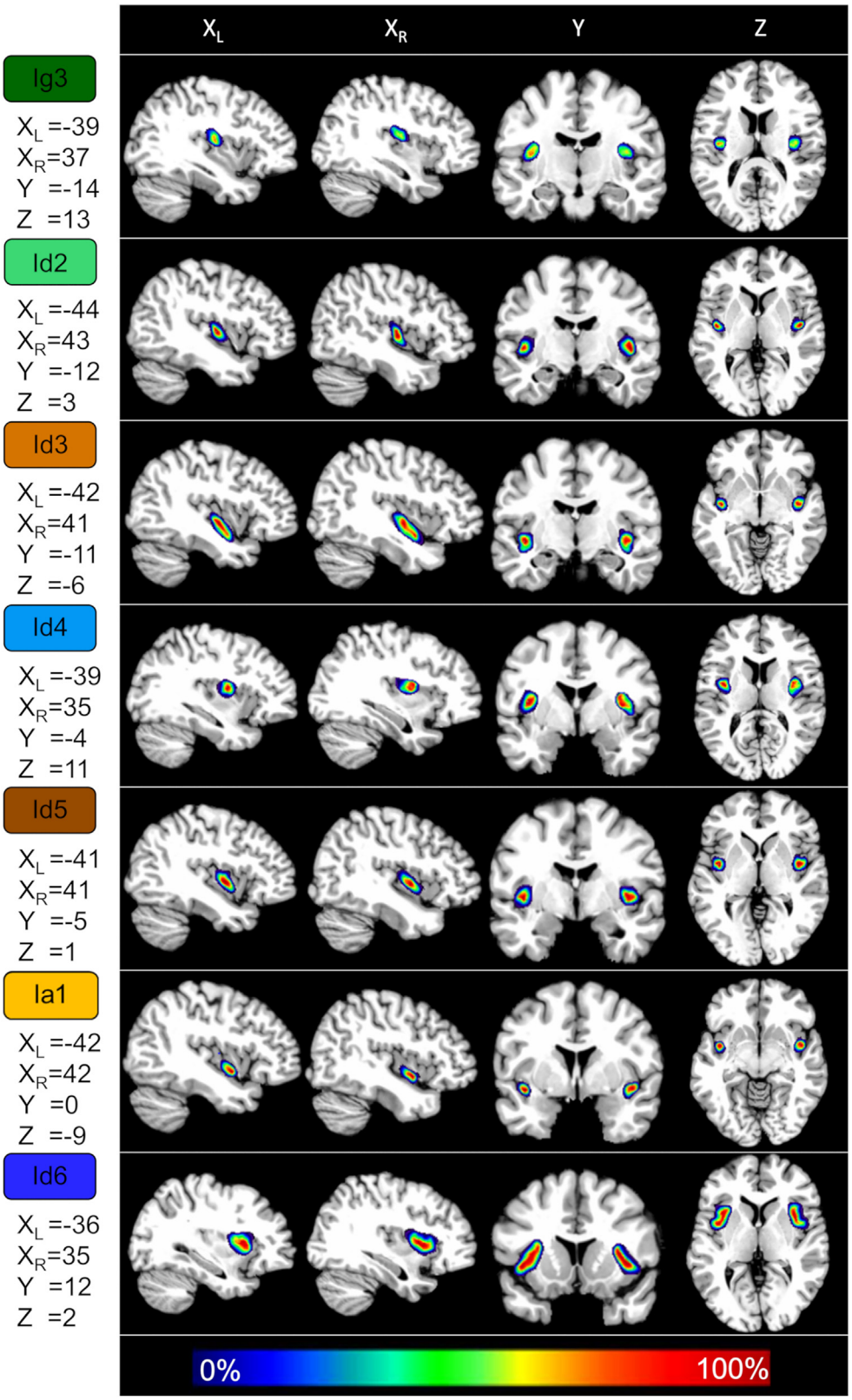

Fig. 12. Probability maps of the seven newly discovered areas of the insular cortex: Ig3, Ia1, Id2, Id3, Id4, Id5 and Id6. The probability is color coded, and ranges from blue (lowest overlap) to red (highest overlap). Stereotactic coordinates of each area are given in the original Colin27 MNI reference space.

domains. This might indicate that there are further microstructural clusters in the posterior insula. A cluster analyses that includes recently published insular areas of the Julich-Brain (e.g. Ia3, DOI: 10.25493/QS00-PJ9) might provide new insights in this context.

Both, MDS and cluster analysis, point out the role of the central sulcus in the human insula as a distinct macro- and microanatomical border reflecting a change in general microstructural composition (Figs. 11 and 14), for which its subdividing role has also been described in functional connectivity studies in infants (Alcauter et al., 2015) and adults (Cauda et al., 2011). Our results could thus add to the early study by Mesulam and Mufson (1985), who described a continuous expansion of the dysgranular sector beyond this macroanatomical landmark, by demonstrating a clear separation into two parts. As Mesulam and Mufson mainly investigated macaque brains, this might reflect differences

Table 4
Coordinates of the centers of gravity of probability maps for each newly discovered area in the insula within the original Colin27-MNI reference space (MNI) and the anatomical MNI space (Amunts et al., 2005).

area	MNI						aMNI					
	left hemisphere			rigth hemisphere			left hemisphere			rigth hemisphere		
	x	y	Z	x	y	z	x	y	z	x	y	z
Ig3	−38	−14	14	38	−14	14	−38	−18	19	38	−18	19
Ia1	−41	−2	−8	43	0	−8	−41	−6	−3	43	−4	−3
Id2	−41	−12	4	42	−10	3	−41	−16	9	42	−14	8
Id3	−41	−8	−9	41	−6	−9	−41	−12	−4	41	−10	−4
Id4	−38	−4	11	39	−3	9	−38	−8	16	39	−7	14
Id5	−40	−3	0	41	−2	0	−40	−7	5	41	−6	5
Id6	−36	10	4	38	11	3	−36	6	9	38	7	8

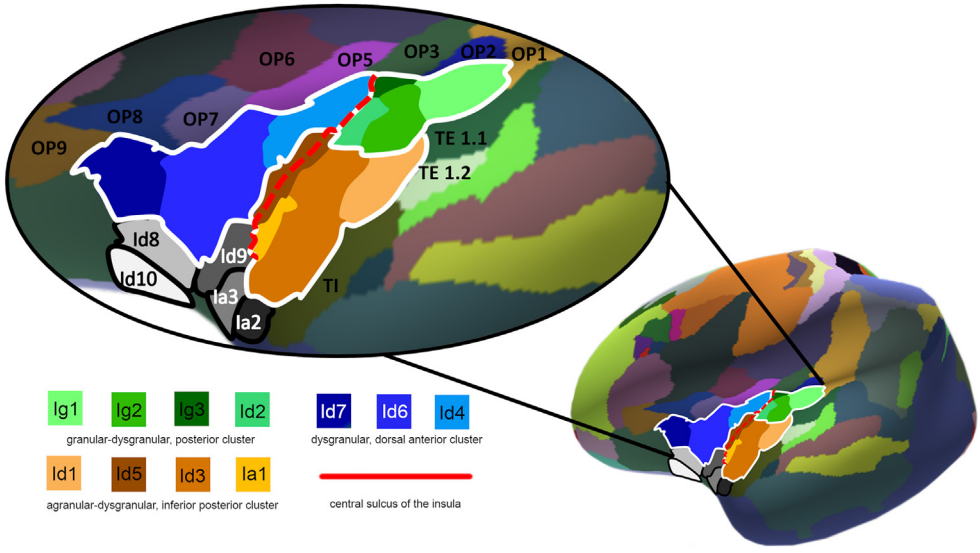

Fig. 13. Maximum probability map (MPM) of seven newly discovered insular areas Ig3, Ia1, Id2,Id3,Id4,Id5 and Id6, as well as previously described areas Ig1, Ig2, Id1 (Kurth et al., 2010) and Id7 (Grodzinsky et al., 2020). The eleven isocortical areas of the human insula can be grouped into a granular-dysgranular, superior posterior cluster, a dysgranular-agranular, inferior posterior cluster and a dysgranular, dorsal anterior cluster. The MPM is reconstructed on the fsaverage template (inflated surface view). Adjacent areas of the ventral anterior insula are not included in this study: Ia2 (DOI: 10.25493/BMNK-B8F), Ia3 (DOI: 10.25493/QS00-PJ9), Id8 (DOI: 10.25493/7QE6-PBE), Id9 (DOI: 10.25493/JMCR-ZNQ), Id10 (DOI: 10.25493/4N71–6SX).

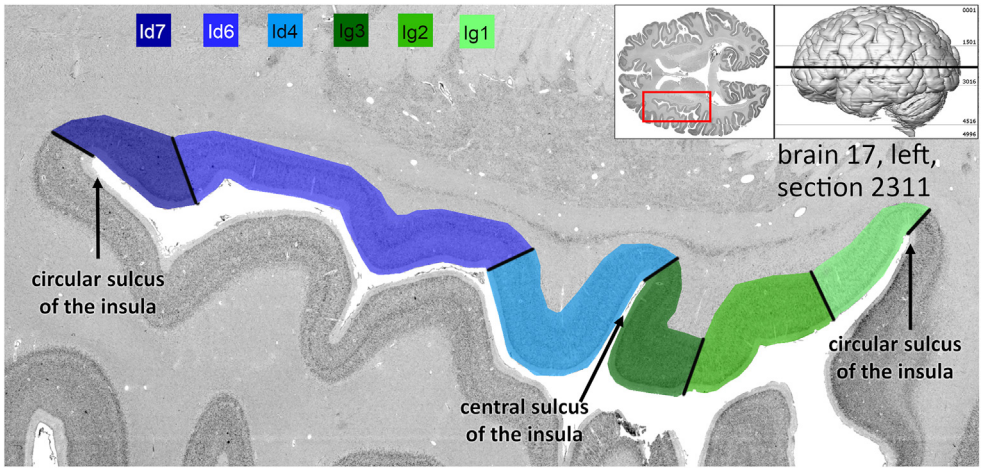

Fig. 14. Topography of the dysgranular areas of the anterior insula and the granular areas of the posterior insula shown on a horizontal section from brain 17. The central sulcus is a distinct microstructural boundary that reflects a general change in the cytoarchitectonic organization of the human insular cortex.

in the insular architecture between species and its function. Because the central sulcus is absent in the macaque insula and it only consists of a smooth surface with one ventral gyrus (Evrard, 2019), the classical cytoarchitectonic sectors (Mesulam and Mufson, 1985) might not be completely transferrable to the human brain. Since the insula differs in shape, extent, gyral and sulcal pattern and cytoarchitectonic composition across species (Buchanan and Johnson, 2011; Butti and Hof, 2010; Shelley and Trimble, 2004), it seems not surprising that microstructural concepts differ amongst primates.

In addition to the results of the cluster analysis, the parcellation of the posterior and dorsal anterior human insula into eleven areas (Fig. 13) provides further evidence for the reassessment of the granular shift and its meaning for this brain region. Similar to other recent parcellations of the insula (Gallay et al., 2012; Morel et al., 2013; Evrard, 2019), we were able to show that while all mapped areas can be classified according to this eponymous concept, each area also consists of determinable cytoarchitectonic features besides this layer IV-related classification (Table 2).Therefore, we come to the conclusion that the granular shift conveys a general principal of cytoarchitectonic organization across areas, but for a more precise description of the insular cytoarchitecture we need to look beyond. Moreover, the multitude of functions is not likely to be reflected microstructurally with one cytoarchitectonic criterion alone.

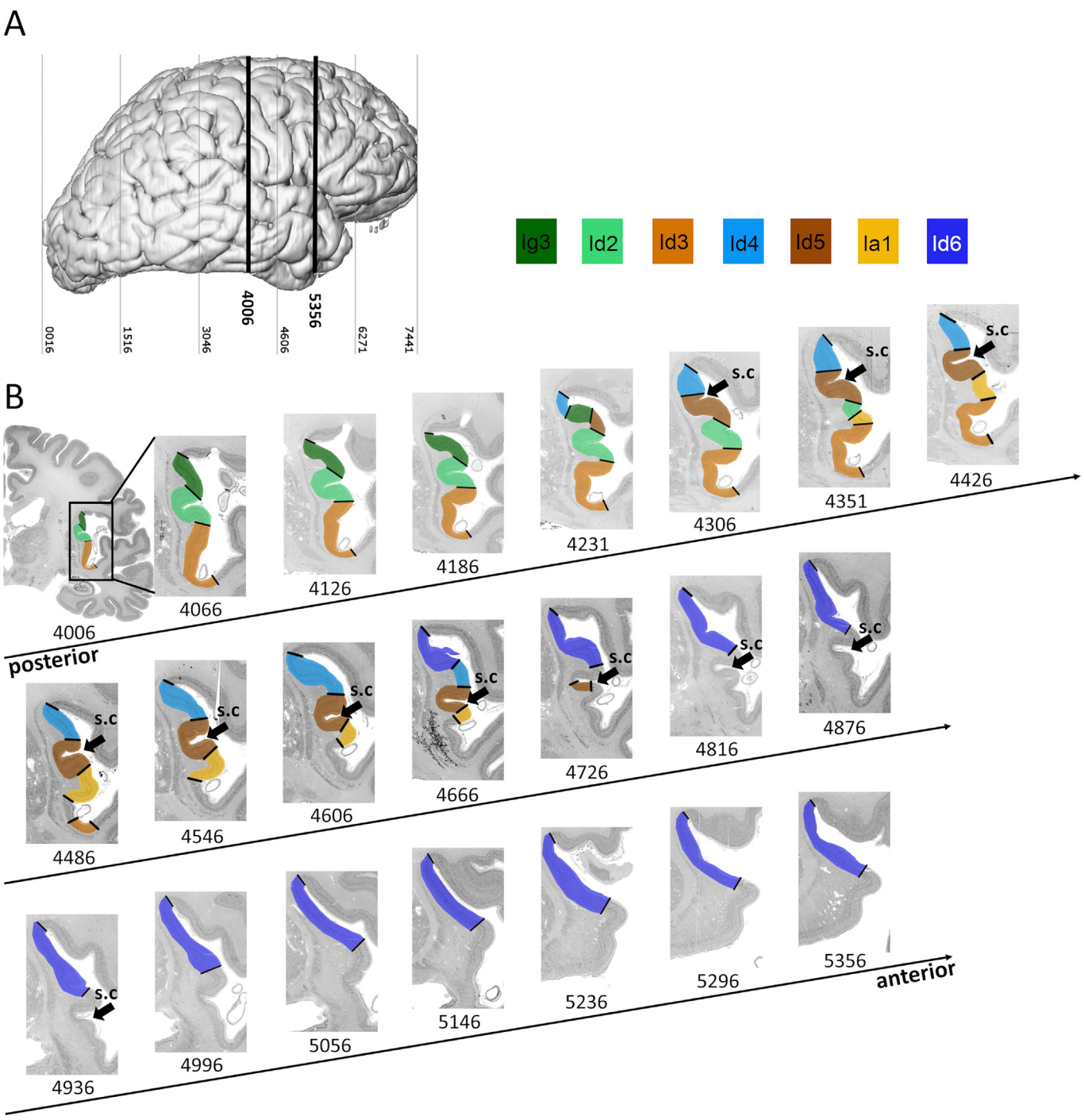

Fig. 15. Topography of seven new areas of the insular cortex in a posterior to anterior sequence of histological coronal sections.

Last but not least our study provides evidence that the microstructural areas can be sharply delineated on a microstructural basis (Figs. 3,4,6,7,8,9), in contrast to some neuroimaging studies, which show that the boundaries of a parcellation can also be gradual rather than clear-cut (Margulies et al., 2016; Tian, 2020). If one looks only at layer IV, the dysgranular areas are no longer sharply delineated but may follow a more gradual distribution. However, if one looks at all six layers in their entirety, as it was done in our study, clear microstructural criteria can be found, which allow, for example, a sharp differentiation between the dysgranular areas. The criteria are summarized in Table 2 and Supplementary 1 provides additional cytoarchitectonic images to show that these distinct characteristics do indeed remain consistent across different brains. It is also important to note that theses neuroimaging studies are on the *meso*/macro scale. Thus, important microstructural features are necessarily blurred due to the lower spatial resolution and transitions between regions may appear as gradients while microstructural analysis shows sharp borders.

4.2. Comparison with other microstructural maps

The concepts of the parcellation of the human insula have been changed during the last decades (Table 5). For example, von Economo and Koskinas (1925) discovered one area in the posterior and four areas in the anterior insula. Brockhaus (1940) characterized a total of 26 ar-

Table 5
Comparison of the present study with other microstructural parcellations of human insular cortex.

authors	microstructural parcellations of the human insula						
	number of areas	areas in anterior/ posterior insula	Localization granular areas	Localization dysgraular areas	localization agranular areas	Superordinated structural groups	Sulcus centralis insulae as microstructurally dividing landmark
Areas as shown in the present study	11*	3 anterior 8 posterior	superior posterior insula	posterior to anterior insula	inferior posterior insula	3 clusters: superior posterior, inferior posterior and dorsal anterior insula	yes
Brodmann (1909)	2	1 anterior 1 posterior	posterior insula	–	anterior insula	–	yes
von Economo and Koskinas (1925)	5	4 anterior 1 posterior	posterior to anterior insula	–	fronto-insular part of anterior insula	–	yes
Rose (1928)	31	5 anterior 26 posterior	posterior to anterior insula	posterior insula	inferior posterior insula	3 regions: agranularis, prope agranularis, granularis	yes
Brockhaus (1940)	26	16 anterior 10 posterior	superior posterior to anterior insula	posterior to anterior insula	inferior anterior insula	3 regions: allocorticalis, mesocorticali, isocorticalis	yes
Mesulam and Mufson (1985)	4	No clear allocation	superior posterior insula	posterior to anterior insula	Inferior posterior to anterior insula	4 sectors: granular, dysgranular, agranular, allocortical	no
Bonthius et al. (2005)	3	No clear allocation	superior posterior insula	posterior to anterior insula	Inferior posterior to anterior insula	3 sectors: granular, dysgranular, agranular	no
Morel et al. (2013)	7	No clear allocation	superior posterior insula	posterior to anterior insula	Inferior posterior to anterior insula	–	no

*ventral anterior insula not included in this study.

eas in the insular cortex, which were grouped into three superordinate domains (allocorticalis, mesocorticali, isocorticalis). Rose (1928) described a total of 31 distinct areas in the human insula. These historical maps agreed on the central sulcus as a macrostructural landmark and described a downgrade of granularity with different degrees. Our data are in accordance with these findings; the present subparcellation into eleven distinct areas seems to be topographically most similar to the map of Brockhaus (1940) among these historical maps.

A recent multi-architectonic histological study detected seven cortical areas (G, Ig, Id1, Id2, Id3, Ia1, Ia2) in the human insula (Morel et al., 2013). Regarding the granular modality, their results indicated at least two types of areas, distinguishable through a change of density and thickness in layer II and IV. The GLI-based approach used in this and previous studies confirmed this finding and detected two granular areas with a wide layer II and IV (Ig1/Ig2) (Kurth et al., 2010b) in contrast to granular area Ig3, comprising a thinner layer II and IV. Dysgranular areas Id1 and Id3 also seem to correspond microstructurally to our dysgranular areas Id2 and Id3. In contrast to the present observations, the study of Morel et al. (2013) did not identify the central sulcus as microanatomical border for the granular and dysgranular modality. While they described an unchanged expansion of G, Ig, Id1, Id2 and Id3 surpassing this landmark, our approach indicated a clear termination of granular and posterior dysgranular areas at the central sulcus. Especially the characteristic anterior dysgranular areas Id4, Id6 and Id7 were therefore not described by Morel et al. (2013).

4.3. Comparison with multimodal studies

The results of the present cluster analysis (Fig. 10A) seem to provide a sound microstructural basis for findings from current imaging studies. Deen et al. (2011) identified a threefold subdivision of the insula in a posterior, dorsal anterior and ventral anterior region by means of a functional connectivity study. Most recently, Menon and colleagues (Menon et al., 2020) were able to demonstrate that the underlying microstructure of these subdivisions differs significantly, using an in vivo ultra-high field MRI approach. Liu et al. (2018) observed altered functional connectivity of these three subregions in Alzheimer's disease patients. The delineation between a posterior, dorsal-anterior and ventral anterior sector is in close accordance with our results. Moreover, Royer et al. (2020) found a ventral anterior to posterior as well as a dorsal anterior to posterior and ventral anterior myeloarchitectonic gradient, using intracortical MRI profiling. They also suggested a higher intensity of the middle compartment in deep cortical layers compared to dorsal anterior and posterior areas, which is consistent with the findings from our cluster analysis (Fig. 10C). In a functional metanalysis, Kurth et al. (2010a) ascribed sensorimotor functions to the posterior to middle insula and olfactory-gustatory functions to the middle insula, while cognitive tasks elicited activation in the dorsal anterior region and social-emotional tasks in the ventral anterior insula. A similar parcellation into a ventral anterior, dorsal anterior, posterior and middle sector was provided by Nomi et al. (2016) considering dynamic functional network connectivity. Taking into account the not included ventral anterior insula the topography of our clusters is in close alignment with this fourfold division and best fits the $k = 4$ cluster solution presented by Kelly et al. (2012) in a study on cluster analysis across imaging modalities. All in all, it seems reasonable that those functional, myeloarchitectonic and connectivity divisions between anterior/posterior and dorsal/ventral anterior insula are accompanied by a change of the microstructural composition. Especially, for the differentiation of a dorsal anterior, middle to inferior posterior and superior posterior subdivision of the insular cortex, our results provide a cytoarchitectonic foundation.

4.4. Potential of the new maps to study structure-function relationships

Since the present maps are available in the MNI reference spaces and in the *fsaverage* space, there is a wide range of applications for

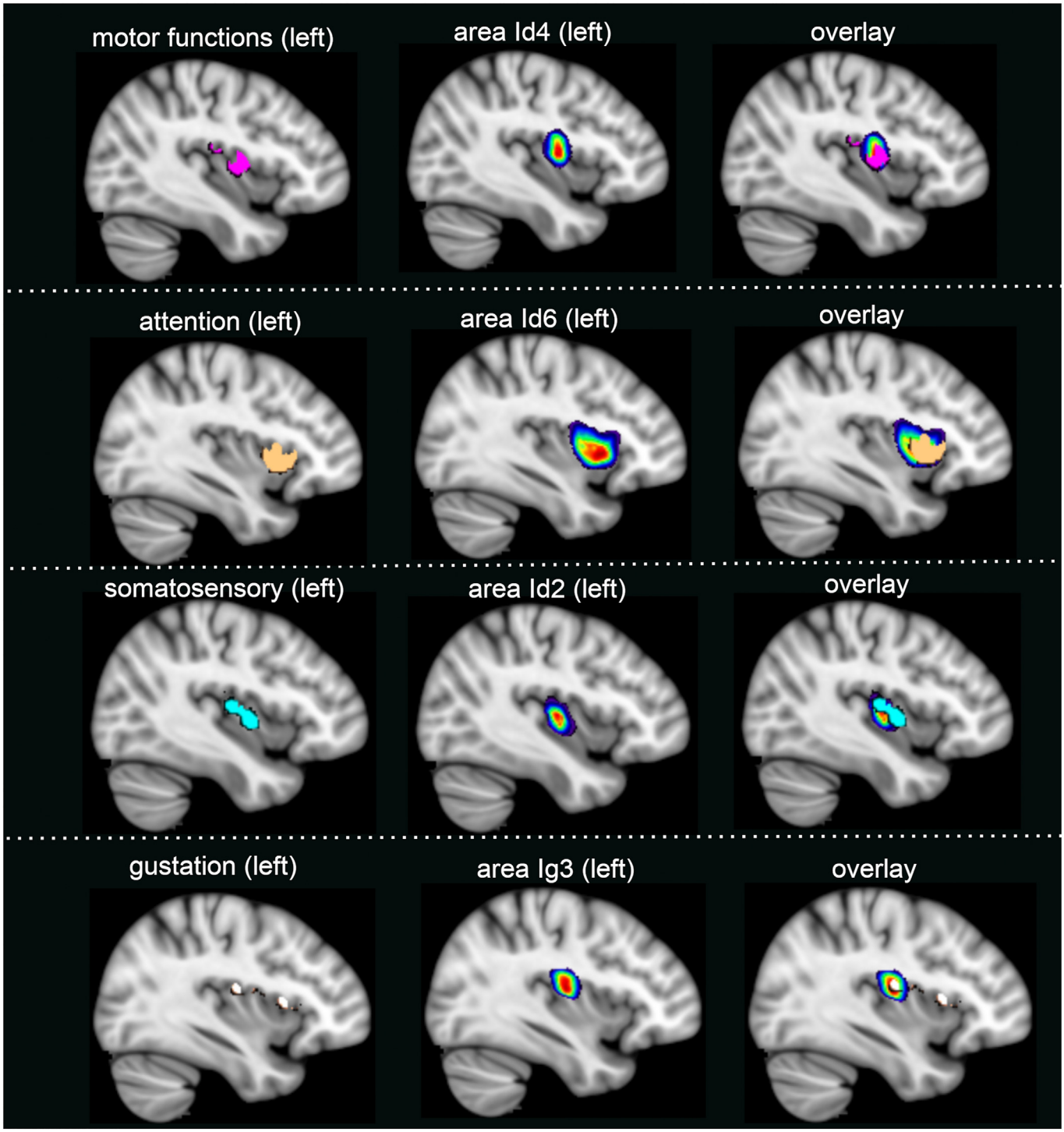

Fig. 16. A comparison between four example areas and the results of a functional meta-analysis (Kurth et al., 2010a) (data downloaded from ANIMA (Reid et al., 2016)). Area Id6 seems to be involved in cognitive functions such as attention, while Id4 is involved in motor tasks. Area Ig3, on the other hand, seems to be activated during gustatory perception, whereas Id2 seems to be active in response to somatosensory stimuli. This example illustrates how our parcellation can be applied to a structure/function comparison.

our microstructural parcellation of the human insular cortex. For instance, the JuBrain Gene Expression (JuGEx) tool (Bludau et al., 2018) enables to analyze differential gene expression with respect to cytoarchitectonic maps. The parcellation could provide the biological basis to study gene expression patterns of the insular cortex in more detail, which seems particularly interesting in the context of its functional and microstructural diversity. The parcellation could also be used as a seed region in studies of functional or structural connectivity (Caspers et al., 2013) to further examine the connection between the insular cortex and other cortical and subcortical structures. The registration in the *fsaverage* space allows an analysis of structural parameters (e.g. cortical thickness) of the insular cortex on a cytoarchitectonic basis, and to visualize the Julich-Brain atlas in the inflated surface view, which is an advantage for areas located in the depths of the brain such as insular areas (Fig. 13). This could lead for example to new insights into the relationship between the structure of the insula and various diseases associated

with this brain region (Namkung et al., 2017; Fathy et al., 2020). Using Freesurfer (Fischl, 2012), one can also examine the areas with respect to sex and hemispheric differences with a larger number of cases. In the present study based on ten brains, significant effects were not found.

Finally, the availability of the microstructural insular areas in a common reference space allows the establishment of a decent structure-function relationship (Eickhoff et al., 2007). The cytoarchitectonic areas could be functionally decoded to determine the approximate function of an area, as it was recently shown for the relationship between logical negation and insular area Id7 (Grodzinsky et al., 2020). Some examples for a possible structural/functional comparison are given in Fig. 16.

5. Conclusion

In conclusion, the microstructure of the insular cortex, as well as its functionality, is characterized by high diversity and a broad range of cytoarchitectonic features. These are by no means limited to laminar IV, but can be found across all six layers. This remarkable diversity and number of microstructural areas might represent the basis for the complex functional organization in this brain region. In addition to the division into clearly distinguishable areas, we were able to demonstrate that these areas can be further grouped into superordinated clusters with similar structure, between which the sulcus centralis insulae forms a distinct microscopic boundary. Study results on functional parcellations and functional connectivity show similar clusters. This suggests that although the insular cortex is a highly variable, multi-functional brain region, it is nevertheless based on an overarching structural/functional organization principle with clear anatomical localization. Since all detected areas of the human insula are available as 3D probability maps in standard MNI space for the first time, the present study provides a quantitative microanatomical basis for further decoding the structural-functional relationship in this complex and functionally dense region of human neocortex.

Declaration of Competing Interest

The authors declare no competing interests.

Credit authorship contribution statement

Julian Quabs: Investigation, Data curation, Formal analysis, Writing – review & editing. **Svenja Caspers:** Data curation, Supervision, Writing – review & editing. **Claudia Schöne:** Investigation. **Hartmut Mohlberg:** Methodology, Software. **Sebastian Bludau:** Formal analysis, Software, Writing – review & editing. **Timo Dickscheid:** Methodology. **Katrin Amunts:** Conceptualization, Data curation, Supervision, Writing – review & editing.

Data availability

The probability maps and the maximum probability maps are publicly and freely available for download at the Julich-Brain atlas (https://jubrain.fz-juelich.de/apps/cytoviewer2/cytoviewer-maintenance.php##mitte) and the Human Brain Project (https://atlases.ebrains.eu/viewer/-/a:juelich:iav:atlas:v1.0.0:1/t:minds:core:referencespace:v1.0.0:tmp-fsaverage/p:minds:core:parcellationatlas:v1.0.0:94c1125b-b87e-45e4-901c-00daee7f2579-290/@:0.0.0.-W000..2_qztu.-8_uv.–2o6B.2_iz3G..23x6..0.0.0..1) Matlab script for multidimensional scaling and bins of microstructural areas as used in our analysis can be downloaded from: https://github.com/JQuab/Insula-cytoarchitecure-.

Ethics statement

The brains of ten subjects were obtained through the body donor program of the Department of anatomy at the University of Duesseldorf. The procedure was approved by an ethical standards committee on human experimentation (#4863).

Funding

This project has received funding from the European Union's Horizon 2020 Research and Innovation Programme under Grant Agreement No. 945539 (HBP SGA3; to KA, SC).

Acknowledgements

The authors would like to thank Ulrich Opfermann-Emmerich and René Hübbers for technical and logistical support.

Supplementary materials

Supplementary material associated with this article can be found, in the online version, at doi:10.1016/j.neuroimage.2022.119453.

References

Alcauter, S., Lin, W., Keith Smith, J., Gilmore, J.H., Gao, W., 2015. Consistent anterior–posterior segregation of the insula during the first 2 years of life. Cereb. Cortex 25, 1176–1187. doi:10.1093/cercor/bht312.

Amunts, K., Armstrong, E., Malikovic, A., Homke, L., Mohlberg, H., Schleicher, A., Zilles, K., 2007. Gender-specific left-right asymmetries in human visual cortex. J. Neurosci. 27, 1356–1364. doi:10.1523/JNEUROSCI.4753-06.2007.

Amunts, K., Kedo, O., Kindler, M., Pieperhoff, P., Mohlberg, H., Shah, N.J., Habel, U., Schneider, F., Zilles, K., 2005. Cytoarchitectonic mapping of the human amygdala, hippocampal region and entorhinal cortex: intersubject variability and probability maps. Anat. Embryol. (Berl.) 210, 343–352. doi:10.1007/s00429-005-0025-5.

Amunts, K., Mohlberg, H., Bludau, S., Zilles, K., 2020. Julich-Brain: a 3D probabilistic atlas of the human brain's cytoarchitecture. Science 369, 988–992. doi:10.1126/science.abb4588.

Amunts, K., Zilles, K., 2015. Architectonic mapping of the human brain beyond brodmann. Neuron 88, 1086–1107. doi:10.1016/j.neuron.2015.12.001.

Avery, J.A., Liu, A.G., Ingeholm, J.E., Riddell, C.D., Gotts, S.J., Martin, A., 2020. Taste quality representation in the human brain. J. Neurosci. 40, 1042–1052. doi:10.1523/JNEUROSCI.1751-19.2019.

Baier, B., zu Eulenburg, P., Geber, C., Rohde, F., Rolke, R., Maihöfner, C., Birklein, F., Dieterich, M., 2014. Insula and sensory insular cortex and somatosensory control in patients with insular stroke: insula and sensory. Eur. J. Pain 18, 1385–1393. doi:10.1002/j.1532-2149.2014.501.x.

Bamiou, D.E., Musiek, F.E., Luxon, L.M., 2003. The insula (Island of Reil) and its role in auditory processing Literature review. Brain Res. Rev. 42, 143–145. doi:10.1016/S0165-0173(03)00172-3.

Bastuji, H., Frot, M., Perchet, C., Magnin, M., Garcia-Larrea, L., 2016. Pain networks from the inside: spatiotemporal analysis of brain responses leading from nociception to conscious perception: pain networks from the inside. Hum. Brain Mapp. 37, 4301–4315. doi:10.1002/hbm.23310.

Bermudez-Rattoni, F., 2014. The forgotten insular cortex: its role on recognition memory formation. Neurobiol. Learn. Mem. 109, 207–216. doi:10.1016/j.nlm.2014.01.001.

Billeke, P., Ossandon, T., Perrone-Bertolotti, M., Kahane, P., Bastin, J., Jerbi, K., Lachaux, J.-P., Fuentealba, P., 2020. Human anterior insula encodes performance feedback and relays prediction error to the medial prefrontal cortex. Cereb. Cortex 30, 4011–4025. doi:10.1093/cercor/bhaa017.

Bludau, S., Eickhoff, S.B., Mohlberg, H., Caspers, S., Laird, A.R., Fox, P.T., Schleicher, A., Zilles, K., Amunts, K., 2014. Cytoarchitecture, probability maps and functions of the human frontal pole. Neuroimage 93, 260–275. doi:10.1016/j.neuroimage.2013.05.052.

Bludau, S., Mühleisen, T.W., Eickhoff, S.B., Hawrylycz, M.J., Cichon, S., Amunts, K., 2018. Integration of transcriptomic and cytoarchitectonic data implicates a role for MAOA and TAC1 in the limbic-cortical network. Brain Struct. Funct. 223, 2335–2342. doi:10.1007/s00429-018-1620-6.

Bonthius, D.J., Solodkin, A., Van Hoesen, G.W., 2005. Pathology of the insular cortex in alzheimer disease depends on cortical architecture. J. Neuropathol. Exp. Neurol. 64, 910–922. doi:10.1097/01.jnen.0000182983.87106.d1.

Bossaerts, P., 2010. Risk and risk prediction error signals in anterior insula. Brain Struct. Funct. 214, 645–653. doi:10.1007/s00429-010-0253-1.

Brockhaus, H., 1940. Die cyto- und myeloarchitektonik des cortex claustralis und des claustrum beim menschen. J. Psychol. Neurol., Leipzig Barth J. A. 49 (4–6).

Brodmann, K., 1909. Vergleichende Lokalisationslehre der Großhirnrinde. Leipz. Barth 343.

Buchanan, K.J., Johnson, J.I., 2011. Diversity of spatial relationships of the claustrum and insula in branches of the mammalian radiation: claustrum and insula diversity in mammals. Ann. N. Y. Acad. Sci. 1225, E30–E63. doi:10.1111/j.1749-6632.2011.06022.x.

Butti, C., Hof, P.R., 2010. The insular cortex: a comparative perspective. Brain Struct. Funct. 214, 477–493. doi:10.1007/s00429-010-0264-y.

Caspers, S., Eickhoff, S.B., Zilles, K., Amunts, K., 2013. Microstructural grey matter parcellation and its relevance for connectome analyses. Neuroimage 80, 18–26. doi:10.1016/j.neuroimage.2013.04.003.

Cauda, F., D'Agata, F., Sacco, K., Duca, S., Geminiani, G., Vercelli, A., 2011. Functional connectivity of the insula in the resting brain. Neuroimage 55, 8–23. doi:10.1016/j.neuroimage.2010.11.049.

Cazzoli, D., Kaufmann, B.C., Paladini, R.E., Müri, R.M., Nef, T., Nyffeler, T., 2021. Anterior insula and inferior frontal gyrus: where ventral and dorsal visual attention systems meet. Brain Commun 3. doi:10.1093/braincomms/fcaa220, fcaa220.

Cera, N., Castelhano, J., Oliveira, C., Carvalho, J., Quinta Gomes, A.L., Peixoto, M.M., Pereira, R., Janssen, E., Castelo-Branco, M., Nobre, P., 2020. The role of anterior and posterior insula in male genital response and in visual attention: an exploratory multimodal fMRI study. Sci. Rep. 10, 18463. doi:10.1038/s41598-020-74681-x.

Chang, L.J., Yarkoni, T., Khaw, M.W., Sanfey, A.G., 2013. Decoding the role of the insula in human cognition: functional parcellation and large-scale reverse inference. Cereb. Cortex 23, 739–749. doi:10.1093/cercor/bhs065.

Craig, A.D., 2003. Interoception: the sense of the physiological condition of the body. Curr. Opin. Neurobiol. 13, 500–505. doi:10.1016/S0959-4388(03)00090-4.

Craig, A.D., Chen, K., Bandy, D., Reiman, E.M., 2000. Thermosensory activation of insular cortex. Nat. Neurosci. 3, 184–190. doi:10.1038/72131.

de Aquino, M.P.B., Verdejo-Román, J., Pérez-García, M., Pérez-García, P., 2019. Different role of the supplementary motor area and the insula between musicians and non-musicians in a controlled musical creativity task. Sci. Rep. 9, 13006. doi:10.1038/s41598-019-49405-5.

Deen, B., Pitskel, N.B., Pelphrey, K.A., 2011. Three systems of insular functional connectivity identified with cluster analysis. Cereb. Cortex 21, 1498–1506. doi:10.1093/cercor/bhq186.

Devlin, J.T., Poldrack, R.A., 2007. In praise of tedious anatomy. Neuroimage 37, 1033–1041. doi:10.1016/j.neuroimage.2006.09.055.

Eickhoff, S.B., Paus, T., Caspers, S., Grosbras, M.-H., Evans, A.C., Zilles, K., Amunts, K., 2007. Assignment of functional activations to probabilistic cytoarchitectonic areas revisited. Neuroimage 36, 511–521. doi:10.1016/j.neuroimage.2007.03.060.

Eickhoff, S.B., Schleicher, A., Zilles, K., Amunts, K., 2006. The human parietal operculum. I. Cytoarchitectonic mapping of subdivisions. Cereb. Cortex 16, 254–267. doi:10.1093/cercor/bhi105.

Eickhoff, S.B., Stephan, K.E., Mohlberg, H., Grefkes, C., Fink, G.R., Amunts, K., Zilles, K., 2005. A new SPM toolbox for combining probabilistic cytoarchitectonic maps and functional imaging data. Neuroimage 25, 1325–1335. doi:10.1016/j.neuroimage.2004.12.034.

Evans, A.C., Janke, A.L., Collins, D.L., Baillet, S., 2012. Brain templates and atlases. Neuroimage 62, 911–922. doi:10.1016/j.neuroimage.2012.01.024.

Evrard, H.C., 2019. The organization of the primate insular cortex. Front. Neuroanat. 13, 43. doi:10.3389/fnana.2019.00043.

Evrard, H.C., Logothetis, N.K., Bud Craig, A.D., 2014. Modular architectonic organization of the insula in the macaque monkey: architectonic organization of macaque insula. J. Comp. Neurol. 522, 64–97. doi:10.1002/cne.23436.

Fathy, Y.Y., Hoogers, S.E., Berendse, H.W., van der Werf, Y.D., Visser, P.J., de Jong, F.J., van de Berg, W.D.J., 2020. Differential insular cortex sub-regional atrophy in neurodegenerative diseases: a systematic review and meta-analysis. Brain Imaging Behav. 14. doi:10.1007/s11682-019-00099-3, 2799–2816.

Fischl, B., 2012. FreeSurfer. NeuroImage 62, 774–781. doi:10.1016/j.neuroimage.2012.01.021.

Fonov, V., Evans, A., McKinstry, R., Almli, C., Collins, D., 2009. Unbiased nonlinear average age-appropriate brain templates from birth to adulthood. Organ. Hum. Brain Mapp. 47, S102. doi:10.1016/S1053-8119(09)70884-5, 2009 Annu. Meet..

Fonov, V., Evans, A.C., Botteron, K., Almli, C.R., McKinstry, R.C., Collins, D.L., 2011. Unbiased average age-appropriate atlases for pediatric studies. Neuroimage 54, 313–327. doi:10.1016/j.neuroimage.2010.07.033.

Frank, S.M., Greenlee, M.W., 2018. The parieto-insular vestibular cortex in humans: more than a single area? J. Neurophysiol. 120, 1438–1450. doi:10.1152/jn.00907.2017.

Gallay, D.S., Gallay, M.N., Jeanmonod, D., Rouiller, E.M., Morel, A., 2012. The insula of reil revisited: multiarchitectonic organization in macaque monkeys. Cereb. Cortex 22, 175–190. doi:10.1093/cercor/bhr104.

Garfinkel, S.N., Seth, A.K., Barrett, A.B., Suzuki, K., Critchley, H.D., 2015. Knowing your own heart: distinguishing interoceptive accuracy from interoceptive awareness. Biol. Psychol. 104, 65–74. doi:10.1016/j.biopsycho.2014.11.004.

Gasquoine, P.G., 2014. Contributions of the insula to cognition and emotion. Neuropsychol. Rev. 24, 77–87. doi:10.1007/s11065-014-9246-9.

Gehrlach, D.A., Dolensek, N., Klein, A.S., Roy Chowdhury, R., Matthys, A., Junghänel, M., Gaitanos, T.N., Podgornik, A., Black, T.D., Reddy Vaka, N., Conzelmann, K.-.K., Gogolla, N., 2019. Aversive state processing in the posterior insular cortex. Nat. Neurosci. 22, 1424–1437. doi:10.1038/s41593-019-0469-1.

Gogolla, N., 2017. The insular cortex. Curr. Biol. 27, R580–R586. doi:10.1016/j.cub.2017.05.010.

Grodzinsky, Y., Deschamps, I., Pieperhoff, P., Iannilli, F., Agmon, G., Loewenstein, Y., Amunts, K., 2020. Logical negation mapped onto the brain. Brain Struct. Funct. 225, 19–31. doi:10.1007/s00429-019-01975-w.

Gundersen, H., Bendtsen, T., Korbo, L., Marcussen, N., Møller, A., Nielsen, K., Nyengaard, J., Pakkenberg, B., Sørensen, F., Vesterby, A., 1988. Some new, simple and efficient stereological methods and their use in pathological research and diagnosis. APMIS Acta Pathol. Microbiol. Immunol. Scand. 96, 379–394. doi:10.1111/j.1699-0463.1988.tb05320.x.

Holmes, C.J., Hoge, R., Collins, L., Woods, R., Toga, A.W., Evans, A.C., 1998. Enhancement of MR images using registration for signal averaging. J. Comput. Assist. Tomogr. 22, 324–333. doi:10.1097/00004728-199803000-00032.

Hömke, L., 2006. A multigrid method for anisotropic PDEs in elastic image registration. Numer. Linear Algebra Appl. 13, 215–229. doi:10.1002/nla.477.

Hu, L., Zhang, L., Chen, R., Yu, H., Li, H., Mouraux, A., 2015. The primary somatosensory cortex and the insula contribute differently to the processing of transient and sustained nociceptive and non-nociceptive somatosensory inputs: cortical processing to somatosensory inputs. Hum. Brain Mapp 36, 4346–4360. doi:10.1002/hbm.22922.

Kelly, C., Toro, R., Di Martino, A., Cox, C.L., Bellec, P., Castellanos, F.X., Milham, M.P., 2012. A convergent functional architecture of the insula emerges across imaging modalities. Neuroimage 61, 1129–1142. doi:10.1016/j.neuroimage.2012.03.021.

Kurth, F., Zilles, K., Fox, P.T., Laird, A.R., Eickhoff, S.B., 2010a. A link between the systems: functional differentiation and integration within the human insula revealed by meta-analysis. Brain Struct. Funct. 214, 519–534. doi:10.1007/s00429-010-0255-z.

Kurth, F., Eickhoff, S.B., Schleicher, A., Hoemke, L., Zilles, K., Amunts, K., 2010b. Cytoarchitecture and probabilistic maps of the human posterior insular cortex. Cereb. Cortex 20, 1448–1461. doi:10.1093/cercor/bhp208.

Lamm, C., Singer, T., 2010. The role of anterior insular cortex in social emotions. Brain Struct. Funct. 214, 579–591. doi:10.1007/s00429-010-0251-3.

Lau, T., Gershman, S.J., Cikara, M., 2020. Social structure learning in human anterior insula. Elife 9, e53162. doi:10.7554/eLife.53162.

Li, Y., Zhang, T., Li, W., Zhang, J., Jin, Z., Li, L., 2020. Linking brain structure and activation in anterior insula cortex to explain the trait empathy for pain. Hum. Brain Mapp 41, 1030–1042. doi:10.1002/hbm.24858.

Limanowski, J., Lopes, P., Keck, J., Baudisch, P., Friston, K., Blankenburg, F., 2019. Action-dependent processing of touch in the human parietal operculum and posterior insula. Cereb. Cortex 30 (2), 607–617. doi:10.1093/cercor/bhz111.

Liu, X., Chen, X., Zheng, W., Xia, M., Han, Y., Song, H., Li, K., He, Y., Wang, Z., 2018. Altered functional connectivity of insular subregions in Alzheimer's disease. Front. Aging Neurosci. 10, 107. doi:10.3389/fnagi.2018.00107.

Livneh, Y., Sugden, A.U., Madara, J.C., Essner, R.A., Flores, V.I., Sugden, L.A., Resch, J.M., Lowell, B.B., Andermann, M.L., 2020. Estimation of current and future physiological states in insular cortex. Neuron 105, 1094–1111. doi:10.1016/j.neuron.2019.12.027, e10.

Loued-Khenissi, L., Pfeuffer, A., Einhäuser, W., Preuschoff, K., 2020. Anterior insula reflects surprise in value-based decision-making and perception. Neuroimage 210, 116549. doi:10.1016/j.neuroimage.2020.116549.

Mahalanobis, P.C., Majumdar, D.N., Rao, C.R., 1949. Anthropometric survey of the United Provinces, 1941: a statistical study. Popul. Fr. Ed. 5, 186. doi:10.2307/1523944.

Margulies, D.S., Ghosh, S.S., Goulas, A., Falkiewicz, M., Huntenburg, J.M., Langs, G., Bezgin, G., Eickhoff, S.B., Castellanos, F.X., Petrides, M., Jefferies, E., Smallwood, J., 2016. Situating the default-mode network along a principal gradient of macroscale cortical organization. Proc. Natl. Acad. Sci. 113, 12574–12579. doi:10.1073/pnas.1608282113.

Mazzola, L., Mauguière, F., Isnard, J., 2019. Functional mapping of the human insula: data from electrical stimulations. Rev. Neurol. 175, 150–156. doi:10.1016/j.neurol.2018.12.003, (Paris).

Menon, V., Gallardo, G., Pinsk, M.A., Nguyen, V.-.D., Li, J.R., Cai, W., Wassermann, D., 2020. Microstructural organization of human insula is linked to its macrofunctional circuitry and predicts cognitive control. Elife 9, e53470. doi:10.7554/eLife.53470.

Menon, V., Uddin, L.Q., 2010. Saliency, switching, attention and control: a network model of insula function. Brain Struct. Funct. 214, 655–667. doi:10.1007/s00429-010-0262-0.

Merker, B., 1983. Silver staining of cell bodies by means of physical development. J. Neurosci. Methods 9, 235–241. doi:10.1016/0165-0270(83)90086-9.

Mesulam, M.M., Mufson, E.J., Peters, A., Jones, E.G., 1985. The insula of reil in man and monkey. In: Association and Auditory Cortices. Springer US, Boston, MA, pp. 179–226. doi:10.1007/978-1-4757-9619-3_5.

Morel, A., Gallay, M.N., Baechler, A., Wyss, M., Gallay, D.S., 2013. The human insula: architectonic organization and postmortem MRI registration. Neuroscience 236, 117–135. doi:10.1016/j.neuroscience.2012.12.076.

Namboodiri, V.M.K., Stuber, G.D., 2020. Interoceptive inception in insula. Neuron 105, 959–960. doi:10.1016/j.neuron.2020.02.032.

Namkung, H., Kim, S.H., Sawa, A., 2017. The insula: an underestimated brain area in clinical neuroscience, psychiatry, and neurology. Trends Neurosci. 40, 200–207. doi:10.1016/j.tins.2017.02.002.

Nieuwenhuys, R., 2012. The insular cortex: a review. Prog. Brain Res. 195, 123–163. doi:10.1016/b978-0-444-53860-4.00007-6.

Nomi, J.S., Farrant, K., Damaraju, E., Rachakonda, S., Calhoun, V.D., Uddin, L.Q., 2016. Dynamic functional network connectivity reveals unique and overlapping profiles of insula subdivisions: dynamic connections of insula subdivisions. Hum. Brain Mapp. 37, 1770–1787. doi:10.1002/hbm.23135.

Oi, H., Hashimoto, T., Nozawa, T., Kanno, A., Kawata, N., Hirano, K., Yamamoto, Y., Sugiura, M., Kawashima, R., 2017. Neural correlates of ambient thermal sensation: an fMRI study. Sci. Rep. 7, 11279. doi:10.1038/s41598-017-11802-z.

Reid, A.T., Bzdok, D., Genon, S., Langner, R., Müller, V.I., Eickhoff, C.R., Hoffstaedter, F., Cieslik, E.C., Fox, P.T., Laird, A.R., Amunts, K., Caspers, S., Eickhoff, S.B., 2016. ANIMA: a data-sharing initiative for neuroimaging meta-analyses. Neuroimage 124, 1245–1253. doi:10.1016/j.neuroimage.2015.07.060.

Rose, M., 1928. Die inselrinde des menschen und der tiere. J. Psychol. Neurol. 37, 467–624.

Royer, J., Paquola, C., Larivière, S., Vos de Wael, R., Tavakol, S., Lowe, A.J., Benkarim, O., Evans, A.C., Bzdok, D., Smallwood, J., Frauscher, B., Bernhardt, B.C., 2020. Myeloarchitecture gradients in the human insula: histological underpinnings and association to intrinsic functional connectivity. Neuroimage 216, 116859. doi:10.1016/j.neuroimage.2020.116859.

Schleicher, A., Amunts, K., Geyer, S., Morosan, P., Zilles, K., 1999. Observer-independent method for microstructural parcellation of cerebral cortex: a quantitative approach to cytoarchitectonics. Neuroimage 9, 165–177. doi:10.1006/nimg.1998.0385.

Schleicher, A., Morosan, P., Amunts, K., Zilles, K., 2009. Quantitative architectural analysis: a new approach to cortical mapping. J. Autism Dev. Disord. 39, 1568–1581. doi:10.1007/s10803-009-0790-8.

Schleicher, A., Palomero-Gallagher, N., Morosan, P., Eickhoff, S.B., Kowalski, T., de Vos, K., Amunts, K., Zilles, K., 2005. Quantitative architectural analysis:

a new approach to cortical mapping. Anat. Embryol. (Berl.) 210, 373–386. doi:10.1007/s00429-005-0028-2.
Segerdahl, A.R., Mezue, M., Okell, T.W., Farrar, J.T., Tracey, I., 2015. The dorsal posterior insula subserves a fundamental role in human pain. Nat. Neurosci. 18, 499–500. doi:10.1038/nn.3969.
Shelley, B.P., Trimble, M.R., 2004. The insular Lobe of Reil–its Anatamico-Functional, behavioural and neuropsychiatric attributes in humans–a review. World J. Biol. Psychiatry 5, 176–200. doi:10.1080/15622970410029933.
Small, D.M., 2010. Taste representation in the human insula. Brain Struct. Funct. 214, 551–561. doi:10.1007/s00429-010-0266-9.
Stephani, C., Fernandez-Baca Vaca, G., Maciunas, R., Koubeissi, M., Lüders, H.O., 2011. Functional neuroanatomy of the insular lobe. Brain Struct. Funct. 216, 137–149. doi:10.1007/s00429-010-0296-3.
Tan, L.L., Pelzer, P., Heinl, C., Tang, W., Gangadharan, V., Flor, H., Sprengel, R., Kuner, T., Kuner, R., 2017. A pathway from midcingulate cortex to posterior insula gates nociceptive hypersensitivity. Nat. Neurosci. 20, 1591–1601. doi:10.1038/nn.4645.
Tian, Y., 2020. Topographic organization of the human subcortex unveiled with functional connectivity gradients. Nat. Neurosci. 23, 26.
Toga, A.W., Thompson, P.M., Mori, S., Amunts, K., Zilles, K., 2006. Towards multimodal atlases of the human brain. Nat. Rev. Neurosci. 7, 952–966. doi:10.1038/nrn2012.
Uddin, L.Q., 2015. Salience processing and insular cortical function and dysfunction. Nat. Rev. Neurosci. 16, 55–61. doi:10.1038/nrn3857.
Uddin, L.Q., Nomi, J.S., Hébert-Seropian, B., Ghaziri, J., Boucher, O., 2017. Structure and function of the human insula. J. Clin. Neurophysiol. 34, 300–306. doi:10.1097/WNP.0000000000000377.
Veldhuizen, M., Nachtigal, D., Teulings, L., Gitelman, D., Small, D., 2010. The insular taste cortex contributes to odor quality coding. Front. Hum. Neurosci. 4. doi:10.3389/fnhum.2010.00058.
Vogt, C., Vogt, O., 1919. Allgemeine ergebnisse unserer hirnforschung. J. Psychol. Neurol. 25 279–262.
von Economo, C., Koskinas, G.N., 1925. Die Cytoarchitektonik der Hirnrinde des Erwachsenen Menschen. Wien Berl. Springer.
Wang, X., Wu, Q., Egan, L., Gu, X., Liu, P., Gu, H., Yang, Y., Luo, J., Wu, Y., Gao, Z., Fan, J., 2019. Anterior insular cortex plays a critical role in interoceptive attention. eLife 8, e42265. doi:10.7554/eLife.42265.
Ward, J.H., 1963. Hierarchical grouping to optimize an objective function. J. Am. Stat. Assoc. 58, 236–244. doi:10.1080/01621459.1963.10500845.
Woolnough, O., Forseth, K.J., Rollo, P.S., Tandon, N., 2019. Uncovering the functional anatomy of the human insula during speech. Elife 8, e53086. doi:10.7554/eLife.53086.
Wree, A., Schleicher, A., Zilles, K., 1982. Estimation of volume fractions in nervous tissue with an image analyzer. J. Neurosci. Methods 6, 29–43. doi:10.1016/0165-0270(82)90014-0.
Zachlod, D., Rüttgers, B., Bludau, S., Mohlberg, H., Langner, R., Zilles, K., Amunts, K., 2020. Four new cytoarchitectonic areas surrounding the primary and early auditory cortex in human brains. Cortex 128, 1–21. doi:10.1016/j.cortex.2020.02.021.
Zilles, K., Amunts, K., 2010. Centenary of Brodmann's map — conception and fate. Nat. Rev. Neurosci. 11, 139–145. doi:10.1038/nrn2776.